NTNU
Norwegian University of
Science and Technology

Voltage tuning of spin and charge supercurrents in a spin-active Josephson Junction

Oda Bolme

MSc in Physics
Submission date: June 2018
Supervisor: Jacob Rune Wüsthoff Linder, IFY

Norwegian University of Science and Technology
Department of Physics

Voltage tuning of spin and charge supercurrents in a spin-active Josephson Junction

Oda Bolme

Supervisor: Jacob Linder
Department of physics
Norwegian Univeristy of Science and Technology

June 5, 2018

Summary

Charge and spin-supercurrents in a spin-active Josephson junction is investigated through the quasiclassical theory of superconductivity. Analytical work has been performed and numerical results are presented, showing that through the application of a voltage bias across the normal metal weal link, the distribution function in the normal metal is brought out of equilibrium and the magnitude of the supercurrents decreases. The transition to a π-junction is controllable via the voltage bias as a consequence.

Preface

This thesis is the result of a two year master programme at The Norwegian University of Science and Technology. The work accounts for 60 ECTS, of which the bulk part of the project took place during the last two semesters of the fall 2017 and spring 2018.

I want to express the gratitude I have for what this work has taught me, and for the people who guided me along the way; I have learned a lot. It has been a challenge, and a good one at that. May I encounter many more like it in the future. To my supervisor: thank you for taking me on as your student, for your insights, and for your patience. To my three sisters: thank you for sharing your strength. To my parents: thank you for your tireless support, and my independence. To the deity: thank you for introducing chaos.

Oda Bolme
May 12, 2018
Trondheim, Norway

Contents

Chapter 1

Introduction

The field of spintronics is one of great interest, both theoretically and experimentally. The growing promise of developing spintronic devices that may drastically improve the storage and frequency capacity of computers has accumulated momentum within condensed matter physics in the past decades[1]. By taking advantage of the electron's spin degree of freedom, the field of spintronics offer a new level of handling data, both with regards to information storage and transfer. As Žutic' et al. presents in ref. [1], the study of spintronics boils down to answering three questions: (1) *what is an effective way to polarize a spin system?* (2) *how long is the system able to remember its spin orientation?* (3) *how can spin be detected?* The work done for this thesis is a humble contribution to the answering of question (1).

Implementing superconductivity into the field of spintronics is interesting due to its capacity to produce supercurrents with long spin lifetimes[2][3], even in non-superconducting materials through the proximity effect[4], offering a solution to the heat dissipation problem in conventional spintronics[5]. It has also been shown that Cooper pairs can be spin-polarized[6][7][8]. Magnetic materials offer ways to produce and control spin effects, and recently, spin-supercurrents were induced in a Josephson junction through magnetic insulators [9]. Establishing an understanding of the physical behavior of the interplay between superconductors, magnetic materials, and by which means their interplay is most efficiently controlled, is crucial. Voltage control of the supercurrent through a Josephson junction was investigated theoretically in 1998[10], around the same time as experimental work was done on the topic [11][12]. The possibility of inducing spin-supercurrents in superconducting-normal metal junctions, and controlling them via non-equilibrium effects through the implementation of a voltage bias has been the motivation behind the work presented in this thesis.

The role of superconductivity in spintronics was first investigated early in the 1970's([13], [14],[15]), even before non-superconducting spin transport was considered[16], and with the discovery of the supercurrents consisting of the spin-triplet Cooper, not only occurring in triplet superconductors[17][18], but also in systems comprised of superconductors in junction with magnetic materials[6][19], is making rise to a new and exciting branch of study within the field spintronics.

The text starts with a short introduction on superconductivity, the proximity effect and many-body theory. It is followed by the more thorough microscopic theory needed for the derivation of the kinetic equation governing the behaviour of the interesting physics of the system under investigation. This is followed by a description of the system and the analytical and numerical results.

1.1 Superconductivity

Conventional superconductivity, discovered by H. K. Onnes in 1911 [20],[21],[22], is a physical phenomenon observed in certain materials when cooled below a threshold temperature, T_c. There are two main behaviours that arise in the superconducting state: the material completely expel any external magnetic field (Meissner effect), discovered in 1933[23], and the material exhibits no electrical resistance. First to conceptualise a theory for superconductivity was Fritz and Heinz London in 1935[24], being especially successful explaining the Meissner effect with their London theory. A few decades later Landau and Ginzburg presented a phenomenological approach, deducing a macroscopic description of superconductivity[25], which was shortly followed up by Bardeen, Cooper and Schrieffer in 1957[26] with the microscopic description of the phenomenon, now known as BCS theory. Further theoretical developments proceeded the BCS-publication, and in 1958, Gor'kov presented the Green's function method of superconductivity[27], which proved to be one of the most powerful approaches to the description of superconductivity.

The disappearance of electrical resistance in the superconducting state is due to the fact that electrons are behaving attractively and pair up in what is called a Cooper Pair [28]. In a lattice of positively charged ions, electrons that are free to move around distort the ions and cause them to vibrate about their equilibrium positions. The quanta of these vibrations are called phonons, which couples to other electrons in the lattice, effectively creating an attractive interaction between the electrons, see Figure 1.1 for a conceptual visualisation of the pairing.

Conventional superconductivity is a cryogenic phenomenon due to the detrimental effect thermal vibrations has on the phonon-electron coupling, effectively making the phonons invisible to the electrons. In addition, it is worth mentioning that a Cooper pair is a continuum of couplings and breakings of a vast number of electrons, and not a particular couple of electrons, and that the supercurrent is the net drift of these couples of electrons through the system. The coherence length ξ_0 of a Cooper pair varies enormously depending on the parameters of the system. For a conventional superconductor, with a moderate amount of impurities, it is in the order of 10 nm.

1.2 Proximity effect

The superconducting proximity effect describes how the nature of a superconductor can act, simply put, contagiously on another material[1] in its immediate proximity. It is observed that the superconducting correlations persists beyond

[1] Here, the other material is referred to as the "normal" material, also denoted N, meaning non-superconductive

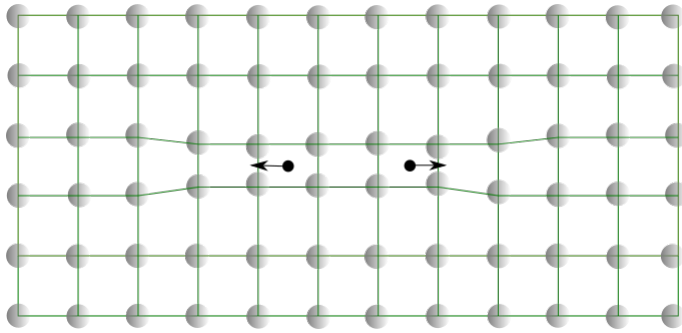

Figure 1.1: Schematic of the distortion of ions in the crystal lattice by the electrons in a Cooper pair.

the interface between the superconductor and the normal material, and a supercurrent can be measured in N. The reverse effect can also occur, where the normal material affects the superconductor and suppresses the superconducting correlations near the interface.

The scattering mechanism that drives the proximity effect is called Andreev reflection. Single electrons in N are blocked from entering the superconductor, but can surpass this by pairing with another electron and transfer into the superconductor as a Cooper pair. This pairing upon transfer into the superconductor is equivalent to the reflection of a hole in N. If N has some kind of magnetic order, the electrons(holes) create a Cooper pair with the centre-of-mass momentum $\pm q$. This spin discrimination causes an oscillation around the singlet spin state, and the result is a mix of singlet and triplet spin states [29]:

$$\begin{aligned} |\uparrow\downarrow\rangle - |\downarrow\uparrow\rangle =& |\uparrow\downarrow\rangle e^{i\boldsymbol{q}\cdot\boldsymbol{r}} - |\downarrow\uparrow\rangle e^{-i\boldsymbol{q}\cdot\boldsymbol{r}} \\ =& \cos(\boldsymbol{q}\cdot\boldsymbol{r})(|\uparrow\downarrow\rangle - |\downarrow\uparrow\rangle) + i\sin(\boldsymbol{q}\cdot\boldsymbol{r})(|\uparrow\downarrow\rangle + |\downarrow\uparrow\rangle) i\sin(\phi)(|\uparrow\downarrow\rangle + |\downarrow\uparrow\rangle) \end{aligned} \tag{1.1}$$

If, in addition to magnetic order, there are spin-rotation mechanisms present, $S_z = \pm 1$ triplet states can be observed.

A different spin-dependent scattering mechanism, driven by magnetically ordered insulators placed in contact with a superconductor, creates similar oscillations around the spin-singlet state. The singlet-triplet combination is brought forth by the magnetic insulators at the interface, and the scattered electrons(holes) tunnel through the insulator and enter the normal material with a spin dependent phase:

$$\begin{aligned} |\uparrow\downarrow\rangle - |\downarrow\uparrow\rangle =& |\uparrow\downarrow\rangle e^{i\phi} - |\downarrow\uparrow\rangle e^{-i\phi} \\ =& \cos(\phi)(|\uparrow\downarrow\rangle - |\downarrow\uparrow\rangle) + i\sin(\phi)(|\uparrow\downarrow\rangle + |\downarrow\uparrow\rangle) \end{aligned} \tag{1.2}$$

The latter scattering mechanism is the one that is implemented in the system investigated in this thesis.

1.3 Quantum theory for many-body systems

When dealing with systems containing many particles ($\sim 10^{20}$)[30], classical physics is deemed impractical. Instead, a quantum approach for many-body systems is preferred, where the system of particles is looked upon as a whole, and the excitations occurring viewed as quasiparticles.

The theory of superconductivity, in particular in relations to other materials is done in terms of Green's functions. They are quantum mechanical propagators, designed in such a way that they are mathematically manageable while still containing interesting information about the system they describe, more on that will be presented in section 2.

1.4 Second quantisation

As mentioned above, when dealing with systems of many particles, and especially when they are indistinguishable, the classical approach is not optimal. Even the first quantised formalism of quantum mechanics is impractical, and so, the theory of superconductivity is presented through the second quantisation. The practicality of this formalism arises from counting the number of particles in each state of the system, and in that way deducing a description of its overall behaviour, rather than tracking each particle individually to thereafter produce a lengthy and awkward description. The systems considered are comprised of many, identical particles, and are therefore invariant under permutation. As a consequence the statistical behaviour of the system differs from that modelled classically. In other words, the statistical degrees of freedom of the system is reduced when the particles are indistinguishable from one another, which introduces the necessity for a more practical and elegant formalism in which many-body systems consequently are described.

Identical particles are divided into two groups: bosons and fermions. Bosons are particles of integer spin, free from the restrictions of the Pauli principle, which allows for more than one particle to occupy a given state and they follow the rules of Bose-Einstein statistics. Fermions have half-integer spin and must obey the Pauli principle and no fermion is found in the same state as another. Fermions follow the statistics of Fermi-Dirac. This produces symmetric and anti-symmetric wavefunctions for bosons and fermions respectively.

The structure of second quantisation is built upon the annihilation operator c_ν and its adjoint in Fock space $c_\nu^\dagger$, annihilating or creating a particle respectively.

For bosons the following commutation relations hold:

$$[c_\nu, c_{\nu'}] = [c_\nu^\dagger, c_{\nu'}^\dagger] = 0, \tag{1.3a}$$
$$[c_\nu, c_{\nu'}^\dagger] = \delta_{\nu\nu'}. \tag{1.3b}$$

Due to their anti-symmetricity, fermions follow similar, but anti-commutation relations:

$$\{c_\nu, c_{\nu'}\} = \{c_\nu^\dagger, c_{\nu'}^\dagger\} = 0, \tag{1.4a}$$
$$\{c_\nu, c_{\nu'}^\dagger\} = \delta_{\nu\nu'}. \tag{1.4b}$$

Without disparaging the role of bosons in the realm of spintronics, further description of their physical and mathematical nature is abandoned, and the ensuing text will focus on fermionic systems, more specifically, systems of electrons.

Expanding the definitions of c_ν and $c_\nu^\dagger$ onto a basis with position $\boldsymbol{r}$ and spin σ states, the following field operators are obtained:

$$\psi_\sigma(\boldsymbol{r}) = \sum_\nu \langle \nu | \boldsymbol{r} \rangle c_{\nu\sigma}, \tag{1.5a}$$
$$\psi_\sigma^\dagger(\boldsymbol{r}) = \sum_\nu \langle \nu | \boldsymbol{r} \rangle c_{\nu\sigma}^\dagger. \tag{1.5b}$$

Following from the anti-commutation relations above, the Fermi field operators obey the same anti-commutation relations:

$$\{\psi_\sigma(\boldsymbol{r}), \psi_{\sigma'}(\boldsymbol{r})\} = \{\psi_\sigma^\dagger(\boldsymbol{r}), \psi_{\sigma'}^\dagger(\boldsymbol{r})\} = 0, \tag{1.6a}$$
$$\{\psi_\sigma(\boldsymbol{r}), \psi_{\sigma'}^\dagger(\boldsymbol{r})\} = \delta_{\sigma\sigma'}\delta(\boldsymbol{r} - \boldsymbol{r'}). \tag{1.6b}$$

To include the spin degrees of freedom of the fermions, and the particle-hole duality, the field operators are from this point onwards defined in the convenient *Nambu-spin* notation:

$$\psi = \begin{pmatrix} \psi_\uparrow \\ \psi_\downarrow \\ \psi_\uparrow^\dagger \\ \psi_\downarrow^\dagger \end{pmatrix}; \qquad \psi^\dagger = \begin{pmatrix} \psi_\uparrow^\dagger & \psi_\downarrow^\dagger & \psi_\uparrow & \psi_\downarrow \end{pmatrix}. \tag{1.7}$$

Chapter 2

The Green's functions

It is necessary to introduce an efficient and suitable way to describe the propagation of particles in the many-body system at hand. This is where the Green's function comes into play. Simply put, it is the overlap between two states of a particle at different times in a time interval[31]:

$$G \sim \langle state|\ \psi(1)\ \psi^\dagger(2)\ |state\rangle, \tag{2.1}$$

where the compact notation $(1) = (\boldsymbol{r}_1, t_1)$ and $(2) = (\boldsymbol{r}_2, t_2)$ is introduced. G is a propagation operator and one can think of the process it describes as adding a particle to a N-particle system, letting it propagate from (1) to (2), and then removing it from the system. The opposite can also be described: where one *removes* a particle from the system, effectively creating a hole, letting the hole propagate from (1) to (2), and then adding the particle back into the system. The Green's function is a way to probe the system under investigation, reading off its properties by looking at the change in behaviour of the added particle or hole.

2.1 The Keldysh Green's function

The Green's function describes a process evolving in time, and is therefore time ordered. This is represented by the time ordering operator, T, in the general definition:

$$G(1,2) = -i\langle T\psi(1)\psi^\dagger(2)\rangle. \tag{2.2}$$

The time ordering can be defined in different ways, depending on the process one wants to describe, and the following time ordered Green's functions can be written out[32]:

$$G_T(1,2) = -i\langle T\psi(1)\psi^\dagger(2)\rangle, \tag{2.3a}$$
$$G_{\tilde{T}}(1,2) = -i\langle \tilde{T}\psi(1)\psi^\dagger(2)\rangle, \tag{2.3b}$$
$$G_>(1,2) = -i\langle \psi(1)\psi^\dagger(2)\rangle, \tag{2.3c}$$
$$G_<(1,2) = i\langle \psi(1)\psi^\dagger(2)\rangle. \tag{2.3d}$$

By suitable linear combinations, these can be compacted into the Keldysh Green's functions[33]:

$$\hat{G}^R(1,2) = -i\Theta(t_1 - t_2)\big\langle\big\{\psi(1), \psi^\dagger(2)\big\}\big\rangle, \tag{2.4a}$$
$$\hat{G}^A(1,2) = i\Theta(t_2 - t_1)\big\langle\big\{\psi(1), \psi^\dagger(2)\big\}\big\rangle, \tag{2.4b}$$
$$\hat{G}^K(1,2) = -i\big\langle\big[\psi(1), \psi^\dagger(2)\big]\big\rangle. \tag{2.4c}$$
$$\tag{2.4d}$$

These are named according to when the creation and annihilation of the particle occurs. G^R is the retarded Green's function and is zero for $t_1 - t_2 < 0$. The advanced Green's function, G^A, is zero for $t_1 - t_2 > 0$. The Keldysh component, G^K describes the non-equilibrium behaviour of the system. The expressions in (2.4) are 4x4 matrices in spin -and particle-hole space, and can be combined in the 8x8 compact matrix form [34]:

$$\check{G}(1,2) = \begin{pmatrix} \hat{G}^R & \hat{G}^K \\ 0 & \hat{G}^A \end{pmatrix}. \tag{2.5}$$

The 8x8 Green's function satisfies the normalisation condition: $\check{G}^2 = \check{1}$, and it is a simple matter to show how that this leads to the following relations: $(\hat{G}^R)^2 = (\hat{G}^A)^2 = \hat{1}$ and $\hat{G}^R\hat{G}^K + \hat{G}^K\hat{G}^A = 0$.

Expanding the Green's function with the *Nambu-spin* notation, defined in eq. (1.7), the general Green's function (2.2) becomes a 4x4 matrix. By definition, this also holds for the retarded, advanced and keldysh Green's functions, and results in matrices with the following structure:

$$\hat{G}^R(1,2) = \begin{pmatrix} \bar{G}^R(1,2) & \bar{F}^R(1,2) \\ (\bar{F}^R)^*(1,2) & (\bar{G}^R)^*(1,2) \end{pmatrix}, \tag{2.6}$$

where the elements are:

$$\bar{G}^R(1,2) = \begin{pmatrix} \psi_\uparrow(1)\psi_\uparrow^\dagger(2) & \psi_\uparrow(1)\psi_\downarrow^\dagger(2) \\ \psi_\downarrow(1)\psi_\uparrow^\dagger(2) & \psi_\downarrow(1)\psi_\downarrow^\dagger(2) \end{pmatrix}, \tag{2.7a}$$
$$\bar{F}^R(1,2) = \begin{pmatrix} \psi_\uparrow(1)\psi_\uparrow(2) & \psi_\uparrow(1)\psi_\downarrow(2) \\ \psi_\downarrow(1)\psi_\uparrow(2) & \psi_\downarrow(1)\psi_\downarrow(2) \end{pmatrix}, \tag{2.7b}$$
$$(\bar{F}^R)^*(1,2) = \begin{pmatrix} ,\psi_\uparrow^\dagger(1)\psi_\uparrow^\dagger(2) & \psi_\uparrow(1)^\dagger\psi_\downarrow^\dagger(2) \\ \psi_\downarrow^\dagger(1)\psi_\uparrow^\dagger(2) & \psi_\downarrow^\dagger(1)\psi_\downarrow^\dagger(2) \end{pmatrix} \tag{2.7c}$$
$$(\bar{G}^R)^*(1,2) = \begin{pmatrix} ,\psi_\uparrow^\dagger(1)\psi_\uparrow(2) & \psi_\uparrow^\dagger(1)\psi_\downarrow(2) \\ \psi_\downarrow^\dagger(1)\psi_\uparrow(2) & \psi_\downarrow^\dagger(1)\psi_\downarrow(2) \end{pmatrix}. \tag{2.7d}$$

From this it becomes obvious why the anomalous Green's functions, $\bar{F}^R(1,2)$ and $(\bar{F}^R)^*(1,2)$, describe the correlations between the electrons and holes in the Cooper pair. They create or annihilate two electrons, whereas the normal Green's functions, $\bar{G}^R(1,2)$ and $(\bar{G}^R)^*(1,2)$, describe the normal, single electron propagation.

Chapter 3

Deriving the Usadel equation

The transport equation for the diffusive, mesoscopic system is called the Usadel equation, and will in the following chapter be derived. The origin of the derivation is the total system Hamiltonian, rising up from microscopic theory. Equations of motion for the field operators and the Green's functions are then found and simplified by the quasiclassical approximation and the "dirty" limit. The derivation presented in this section follows the works of G. D. Mahan[32], J. P. Morten[35] and M. Amundsen[36].

3.1 The electron-phonon interaction

First, the electron-phonon interaction is considered. The superconductor is modelled as a crystal lattice of positively charged ions. An ion j is cited at position $\boldsymbol{R}_j^0$, and oscillates with a deviation $\boldsymbol{Q}_j(t)$ about this equilibrium position when disturbed. The ion's general position is then $\boldsymbol{R}_j = \boldsymbol{R}_j^0 + \boldsymbol{Q}_j(t)$, and the following Hamiltonian is used to describe the interaction [32]:

$$H = \underbrace{\sum_{\boldsymbol{k}\lambda} \omega_{\boldsymbol{k}\lambda} a^\dagger_{\boldsymbol{k}\lambda} a_{\boldsymbol{k}\lambda}}_{\text{Phonons}} + \underbrace{\sum_i \left[\frac{p_i^2}{2m} + \frac{e^2}{2} \sum_{j \neq i} \frac{i}{r_{ij}} \right]}_{\text{Eletrons}} + \underbrace{H_{ei}}_{\text{Electron - ion}} . \tag{3.1}$$

The free phonons are characterised by their frequency $\omega_{\boldsymbol{k}\lambda}$, where $\boldsymbol{k}$ is the wavevector and λ is the polarisation. $a_{\boldsymbol{k}\lambda}$ and $a^\dagger_{\boldsymbol{k}\lambda}$ are the phonon annihilation and creation operators respectively. The second part of eq. (3.1) contains the kinetic term for the individual electron i and the Coulomb interaction between the electrons at cite i and j. H_{el-ion} denotes the interaction between the electrons and ions, defined as:

$$H_{ei} = \sum_{ij} V_{ei}(\boldsymbol{r}_i - \boldsymbol{R}_j), \tag{3.2a}$$

$$= \sum_{ij} V_{ei}(\boldsymbol{r}_i - \boldsymbol{R}_j^{(0)} + \boldsymbol{Q}_j), \tag{3.2b}$$

$$= V_{ei}(\boldsymbol{r}_i - \boldsymbol{R}_j^{(0)}) - \boldsymbol{Q}_j \cdot \nabla V_{ei}(\boldsymbol{r}_i - \boldsymbol{R}_j^{(0)}) + O(Q^2), \tag{3.2c}$$

where the displacement $\boldsymbol{Q}_j$ is assumed to be small, and is power expanded in the last line. The first term in (3.2c) is the electron-ion interaction when the ions are located in their equilibrium positions, this is the chemical potential of the crystal. The non-equilibrium dynamics of the electron-ion interaction is described by the second and third terms in (3.2c), and only the first order term in Q is kept in this derivation. Phonons are the quantised vibrations of the ions, and hence the second term in (3.2c) is the electron-phonon interaction. The electron-phonon interaction is then defined:

$$V_{ep}(\boldsymbol{r}) = \sum_j \boldsymbol{Q}_j \cdot \nabla V_{ei}(\boldsymbol{r}_i - \boldsymbol{R}_j^{(0)}), \tag{3.3}$$

which can be written in terms of its Fourier Transform:

$$V_{ei}(\boldsymbol{r}) = \frac{1}{N}\sum_q V_{ei}(\boldsymbol{q})\mathrm{e}^{i\boldsymbol{q}\cdot\boldsymbol{r}}, \tag{3.4a}$$

$$\nabla V_{ei}(\boldsymbol{r}) = \frac{i}{N}\sum_q \boldsymbol{q} V_{ei}(\boldsymbol{q})e^{i\boldsymbol{q}\cdot\boldsymbol{r}}. \tag{3.4b}$$

Summarising the terms obtained so far:

$$V_{ep}(\boldsymbol{r}) = \frac{i}{N}\sum_q V_{ei}(\boldsymbol{q})e^{i\boldsymbol{q}\cdot\boldsymbol{r}}\boldsymbol{q}\cdot\Big(\sum_j \boldsymbol{Q}_j e^{-i\boldsymbol{q}\cdot\boldsymbol{R}_j^{(0)}}\Big). \tag{3.5a}$$

The displacement vector $\boldsymbol{Q}_j$ can be expanded in the following way[32]:

$$\boldsymbol{Q}_j(t) = \sum_{\boldsymbol{k},\lambda}\big(\frac{\hbar}{2MN\omega_{\boldsymbol{k}\lambda}}\big)^{1/2}\xi_{\boldsymbol{k},\lambda}(a_{\boldsymbol{k},\lambda}\mathrm{e}^{-\omega_{\boldsymbol{k}\lambda}t} + a^\dagger_{-\boldsymbol{k},\lambda}\mathrm{e}^{\omega_{\boldsymbol{k}\lambda}t})\mathrm{e}^{i\boldsymbol{k}\cdot\boldsymbol{R}_j^{(0)}}, \tag{3.6}$$

were M is the ion mass, N is the number of ions in the lattice. Since $\boldsymbol{Q}_j(t)$ represents a displacement in real space, it is equal to its Hermitian conjugate: $\boldsymbol{Q}_j^\dagger = \boldsymbol{Q}_j$. This is true when the following property for the polarisation vector $\xi_{\boldsymbol{k},\lambda}$ holds:

$$\xi^*_{\boldsymbol{k},\lambda} = -\xi_{-\boldsymbol{k},\lambda}. \tag{3.7}$$

It can be shown that:

$$\frac{i}{N}\sum_j \boldsymbol{Q}_j\mathrm{e}^{-\boldsymbol{q}\cdot\boldsymbol{R}_j^{(0)}} = \frac{i}{\sqrt{N}}\sum_{\boldsymbol{G}}\boldsymbol{Q}_{\boldsymbol{q}+\boldsymbol{G}} \tag{3.8a}$$

$$= -\sum_{\boldsymbol{G}}\big(\frac{\hbar}{2MN\omega_{\boldsymbol{k}\lambda}}\big)^{1/2}\xi_{\boldsymbol{q}+\boldsymbol{G}}(a_{\boldsymbol{q}} + a^\dagger_{\boldsymbol{q}}), \tag{3.8b}$$

where $\boldsymbol{G}$ is the reciprocal vector of the solid. $\boldsymbol{q}+\boldsymbol{G}$ is defined within the first Brillouin zone, whereas $\boldsymbol{q}$ can take on values outside it. Simplifying the notation, with $MN = \rho\nu$, ρ being the density of the solid, the interaction Hamiltonian is:

$$V_{ep}(\boldsymbol{q}) = -\sum_{\boldsymbol{qG}} e^{i\boldsymbol{r}\cdot(\boldsymbol{q}+\boldsymbol{G})} V_{ei}(\boldsymbol{q}+\boldsymbol{G})(\boldsymbol{q}+\boldsymbol{G})\cdot\xi_{\boldsymbol{q}}\big(\frac{\hbar}{2\rho\nu\omega_{\boldsymbol{q}}}\big)^{1/2}(a_{\boldsymbol{q}}+a^{\dagger}_{\boldsymbol{q}}). \tag{3.9}$$

The Hamiltonian for the electron-phonon interaction is from eq. (3.9) obtained by integrating the interaction potential over the charge density of the crystal $\rho(\boldsymbol{r})$:

$$H_{ep} = \int d^3r\rho(\boldsymbol{r})V_{ep}(\boldsymbol{r}) \tag{3.10a}$$

$$= -\sum_{\boldsymbol{qG}} \rho(\boldsymbol{q}+\boldsymbol{G})V_{ei}(\boldsymbol{q}+\boldsymbol{G})(\boldsymbol{q}+\boldsymbol{G})\cdot\xi_{\boldsymbol{q}}\big(\frac{\hbar}{2\rho\nu\omega_{\boldsymbol{q}}}\big)^{1/2}(a_{\boldsymbol{q}}+a^{\dagger}_{\boldsymbol{q}}), \tag{3.10b}$$

where $\rho(\boldsymbol{q})$ is defined[32]:

$$\rho(\boldsymbol{q}) = \sum_{\boldsymbol{k}\sigma} c^{\dagger}_{\boldsymbol{k}+\boldsymbol{q}\sigma}c_{\boldsymbol{k}\sigma}. \tag{3.11}$$

Simplifying further we end up with the electron-phonon term:

$$H_{ep} = \sum_{\boldsymbol{qGk}\sigma} M_{\boldsymbol{q}+\boldsymbol{G}}c^{\dagger}_{\boldsymbol{k}+\boldsymbol{q}\sigma}c_{\boldsymbol{k}\sigma}(a_{\boldsymbol{q}}+a^{\dagger}_{\boldsymbol{q}}), \tag{3.12}$$

where

$$M_{\boldsymbol{q}+\boldsymbol{G}} = \big(\frac{\hbar}{2\rho\nu\omega_{\boldsymbol{q}}}\big)^{1/2}\xi_{\boldsymbol{q}}\cdot(\boldsymbol{q}+\boldsymbol{G})V_{ep}(\boldsymbol{q}+\boldsymbol{G}). \tag{3.13}$$

The electron phonon interaction can be described as an electron ($\boldsymbol{k_1}$) moving in the lattice of ions, creating a phonon of momentum $\boldsymbol{q}$, resulting in the electron transitioning to a new state, $\boldsymbol{k'_1} = \boldsymbol{k_1} - \boldsymbol{q}$. Another electron ($\boldsymbol{k_2}$), eventually forming the second half of the Cooper pair, absorbs the phonon and transitions into the state $\boldsymbol{k'_2}$, i.e. the two independent electrons interacted attractively with one another through an exchange of a phonon and hence, the two electron-phonon interaction can be seen as the effective electron-electron interaction.

The state transition from $\boldsymbol{k}_1$ to $\boldsymbol{k'_1}$ causes an oscillation of the local electron density, with frequency $\omega = (\varepsilon_{\boldsymbol{k}1} - \varepsilon_{\boldsymbol{k}1'})/\hbar$, with $\varepsilon_{\boldsymbol{k}1}$ and $\varepsilon_{\boldsymbol{k}1'}$ being the electron energies in the two states $\boldsymbol{k_1}$ and $\boldsymbol{k'_1}$. The ions in the immediate proximity will accumulate towards the increase in electron density. This (now positive) accumulation of ions, attracts the second electron, however, only if the lattice vibrations are in phase with the electron density oscillations[37]. In addition, this attractive interaction is also limited by the characteristic frequency of the ions, called the

Debye frequency, ω_D. Consequently, the condition for attractive interaction between the electrons in the lattice is that $\omega < \omega_D$.

With this properly in place, the BCS interaction potential, V_{kq}[38], is introduced:

$$V_{kq} = \underbrace{\frac{4\pi e^2}{q^2 + \lambda^2}}_{\text{Coulomb interaction}} + \underbrace{\frac{2\hbar\omega_q |M_q|^2}{(\varepsilon_{\boldsymbol{k_1}} - \varepsilon_{\boldsymbol{k_1'}})^2 - (\hbar\omega_q)^2}}_{\text{Frolich interaction}}, \tag{3.14}$$

where M_q is the electron-phonon coupling, and ω_q is the phonon oscillation frequency. In a normal non-superconducting metals is dominated by the Coulomb-term, becoming a positive term, i.e. describing a repulsive interaction. In superconducting materials, V_{kq} is dominated by the Frolich-term and becomes negative, i.e. describing an attractive interaction.

3.2 BCS theory

At this point of the derivation BCS theory comes into play. It offers to simplify the model of superconductivity by using a simple attractive potential:

$$V_{BCS} = \begin{cases} -V_0, & \omega \leq \omega_D \\ 0, & \text{otherwise,} \end{cases} \tag{3.15a}$$

which holds for superconductors with weak electron-phonon coupling [28]. ω_D is the Debye cut-off frequency.

Most of the electrons in the crystal are contained in the Fermi sea. These electrons are of energies below the Fermi energy, E_F, giving rise to the chemical potential of the solid. Apart from that they are inactive in this model. The electrons with energies around E_F are not part of the Fermi sea and are free to roam around as they like. It is assumed that the attraction between the electrons in the Cooper pair is between two electrons of equal and opposite momentum. There are several ways of defending this assumption: the lowest energy state of the pair is the one with zero net momentum [20]. It can also be explained by a more intuitive picture, where the attraction between the electrons is strongest when they are close to each other, or rather, close to the accumulation of positively charged ions caused by the other electron. This is most effective when they travel on the same path, but in opposite direction. The electrons in conventional superconductivity obey the Pauli principle, and the Cooper pairs contain electrons of opposite spins. With these constraints the Hamiltonian for the superconductivity can be defined:

$$H_{BCS} = -V_0 \sum_{\sigma} \int d\boldsymbol{r} \psi_{\sigma}^{\dagger}(1) \psi_{-\sigma}^{\dagger}(1) \psi_{\sigma}(1) \psi_{-\sigma}(1) \tag{3.16}$$

Introducing the order parameter $\Delta(\boldsymbol{r})$:

$$\Delta(\boldsymbol{r}) = \lambda(\boldsymbol{r})\langle\psi_\uparrow(1)\psi_\downarrow(1)\rangle, \tag{3.17}$$

where $\langle ...\rangle$ denotes taking the average value, and $\lambda(\boldsymbol{r})$ is only non-zero inside the bulk superconductor. $\Delta(\boldsymbol{r})$ describes the superconducting correlations of the electrons and holes in the system. By the argument that the deviations from the average, δ, are small (second order and higher terms are omitted), expanding the pairs of field operators from eq.(3.16) :

$$\psi_\uparrow(1)\psi_\downarrow(1) = \Delta(\boldsymbol{r}) + (\psi_\uparrow(1)\psi_\downarrow(1) - \Delta(\boldsymbol{r})) = \Delta(\boldsymbol{r}) + \delta(\boldsymbol{r}) \tag{3.18a}$$

$$\psi^\dagger_\uparrow(1)\psi^\dagger_\downarrow(1) = \Delta^*(\boldsymbol{r}) + (\psi^\dagger_\uparrow(1)\psi^\dagger_\downarrow(1) - \Delta^*(1)) = \Delta^*(\boldsymbol{r}) + \delta^*(\boldsymbol{r}) \tag{3.18b}$$

one can write the H_{BCS} from eq. (3.16) in terms of $\Delta(\boldsymbol{r})$ and $\Delta^*(\boldsymbol{r})$:

$$H_{BCS} = \int d\boldsymbol{r}[\Delta(\boldsymbol{r})\psi^\dagger_\uparrow(\boldsymbol{r_1},t)\psi^\dagger_\downarrow(\boldsymbol{r_1},t) + \Delta^*(\boldsymbol{r})\psi_\downarrow(\boldsymbol{r_1},t)\psi_\uparrow(\boldsymbol{r_1},t)] \tag{3.19}$$

3.3 Impurities

Impurities are an intrinsic part of any physical system. They are accounted for by including an impurity term in the Hamiltonian, H_{imp}[6]:

$$H_{imp} = \sum_\sigma \int d\boldsymbol{r}\ \psi^\dagger_\sigma(1)V_{imp}\psi_\sigma(1) \tag{3.20}$$

Electrons scatter off these impurities, and their direction is affected. Their spin is assumed to be unchanged after a scattering event.

3.4 Equation of motion for the field operators

By the use the Heisenberg equation:

$$i\hbar\partial_t\psi(\boldsymbol{r_1},t) = [\psi(\boldsymbol{r_1},t), H], \tag{3.21}$$

the equation of motion for the field operators $\psi_\sigma(\boldsymbol{r_1},t)$ and $\psi^\dagger_\sigma(\boldsymbol{r_1},t)$ can obtained. Writing out the total Hamiltonian: $H = H_0 + H_{imp} + H_{BCS}$, and running them through (3.21) gives:

$$
\begin{aligned}
[\psi_\sigma(\boldsymbol{r_1},t), H_0 + H_{imp}] &= \sum_{\sigma'} \int d\boldsymbol{r_2} \left[\psi_\sigma(\boldsymbol{r_1},t), \psi^\dagger_{\sigma'}(\boldsymbol{r_2},t)\, H_{sim}(\boldsymbol{r_2},t)\, \psi_{\sigma'}(\boldsymbol{r_2},t)\right] \\
&= \sum_{\sigma'} \int d\boldsymbol{r_2} \Big(\big\{\psi_\sigma(\boldsymbol{r_1},t), \psi^\dagger_{\sigma'}(\boldsymbol{r_2},t)\big\}\, H_{sim}(\boldsymbol{r_2},t)\, \psi_{\sigma'}(\boldsymbol{r_2},t) \\
&\quad - \psi^\dagger_{\sigma'}(\boldsymbol{r_2},t)\big\{\psi_\sigma(\boldsymbol{r_1},t), H_{sim}(\boldsymbol{r_2},t)\psi_{\sigma'}(\boldsymbol{r_1},t)\big\}\Big) \\
&= \sum_{\sigma'} \int \Big(\delta_{\sigma\sigma'}\delta(\boldsymbol{r_1}-\boldsymbol{r_2}) H_{sim}(\boldsymbol{r_2},t)\psi_{\sigma'}(\boldsymbol{r_2},t) \\
&\quad - \psi^\dagger_{\sigma'}(\boldsymbol{r_2},t) H_{sim}(\boldsymbol{r_2},t)\big\{\psi_\sigma(\boldsymbol{r_1},t), \psi_{\sigma'}(\boldsymbol{r_2},t)\big\}\Big) \\
&= H_{sim}(\boldsymbol{r_1},t)\psi_\sigma(\boldsymbol{r_1},t),
\end{aligned}
\tag{3.22}
$$

where H_{sim} is used for the collected single-body terms:

$$
H_{sim} = -\frac{1}{2m}\big(\nabla - ie\boldsymbol{A}(\boldsymbol{r},t)\big)^2 + V_{imp}(\boldsymbol{r}). \tag{3.23}
$$

For the BCS-term, following the same approach as in (3.22):

$$
\begin{aligned}
[\psi_\sigma(\boldsymbol{r_1},t), H_{BCS}] &= \int d\boldsymbol{r_2} \big[\psi_\sigma(\boldsymbol{r_1},t), \Delta^*(\boldsymbol{r_2},t)\psi_\uparrow(\boldsymbol{r_2},t)\psi_\downarrow(\boldsymbol{r_2},t) \\
&\qquad + \Delta(\boldsymbol{r_2},t)\psi^\dagger_\downarrow(\boldsymbol{r_2},t)\psi^\dagger_\uparrow(\boldsymbol{r_2},t)\big] \\
&= \int d\boldsymbol{r_2} \Big(\{\psi_\sigma(\boldsymbol{r_1},t), \psi_\downarrow(\boldsymbol{r_2},t)\}\Delta^*(\boldsymbol{r_2},t)\psi_\uparrow(\boldsymbol{r_2},t) \\
&\qquad - \psi_\downarrow(\boldsymbol{r_2},t)\Delta^*(\boldsymbol{r_2},t)\{\psi_\sigma(\boldsymbol{r_1},t), \psi^\dagger_\downarrow(\boldsymbol{r_2},t)\}\Big) \\
&= \int d\boldsymbol{r_2} \Big(\delta_{\sigma\uparrow}\delta(\boldsymbol{r_1}-\boldsymbol{r_2})\Delta(\boldsymbol{r_2},t)\psi^\dagger_\downarrow(\boldsymbol{r_2},t) \\
&\qquad - \psi^\dagger_\uparrow(\boldsymbol{r_2},t)\Delta(\boldsymbol{r_2},t)\delta_{\sigma\downarrow}\delta(\boldsymbol{r_1}-\boldsymbol{r_2})\Big) \\
&= \delta_{\sigma\uparrow}\Delta(\boldsymbol{r_1},t)\psi^\dagger_\downarrow(\boldsymbol{r_1},t) - \delta_{\sigma\downarrow}\Delta(\boldsymbol{r_1},t)\psi^\dagger_\uparrow(\boldsymbol{r_1},t).
\end{aligned}
\tag{3.24}
$$

The result in Nambu-spin space is:

$$
\begin{aligned}
i\hbar\partial_t\hat{\rho}_3\psi(\boldsymbol{r_1},t) &= \hat{H}(\boldsymbol{r_1},t)\psi(\boldsymbol{r_1},t) \\
&= \big(\frac{1}{2m}(\boldsymbol{p}\hat{1} + \boldsymbol{A}\hat{\rho}_3)^2 + V_{imp}(\boldsymbol{r})\hat{1} - \mu\hat{1} - \hat{\Delta}\big)\psi(\boldsymbol{r},t).
\end{aligned}
\tag{3.25}
$$

The same goes for $\psi^\dagger(\boldsymbol{r_1},t)$ [36]:

$$\begin{aligned} i\hbar\psi^\dagger(\boldsymbol{r_1},t) &= -\psi^\dagger(\boldsymbol{r_1},t)\hat{H}^\dagger(\boldsymbol{r_1},t) \\ &= \psi^\dagger(\boldsymbol{r_1},t)\big(\frac{1}{2m}(\boldsymbol{p}\hat{1}+\boldsymbol{A}\hat{\rho}_3)^2+\hat{1}V_{imp}(\boldsymbol{r})-\mu\hat{1}-\hat{\Delta}\big), \end{aligned} \tag{3.26}$$

where $\hat{\Delta}$ is the matrix:

$$\hat{\Delta} = \begin{pmatrix} 0 & 0 & 0 & \Delta \\ 0 & 0 & -\Delta & 0 \\ 0 & \Delta^* & 0 & 0 \\ -\Delta^* & 0 & 0 & 0 \end{pmatrix}. \tag{3.27}$$

3.5 The equations of motion for the Green's functions

To obtain the equation of motion for the Green's function, the definitions from eq. (2.4) is considered. The retarded component, G^R is considered, and by applying $i\hbar\partial_t\hat{\rho}_3$, from the left and right, the result is:

$$(i\hbar\partial_t\hat{\rho}_3 G^R(1,2))_{ij} = \delta_{ij}\delta(1-2) + (\hat{H}(1)\hat{G}^R(1,2))_{ij} \tag{3.28a}$$

$$\big(G^R(1,2)(-i\hbar\partial_t\hat{\rho}_3)\big)_{ij} = \delta_{ij}\delta(1-2) + (\hat{G}^R(1,2)(\hat{H}^\dagger(2))_{ij} \tag{3.28b}$$

See Appendix A for the detailed calculation of eq. (3.28a) and (3.28b). The equations of motion for the retarded Green's function are:

$$\big(i\partial_{t_1}\hat{\rho}_3 - \hat{H}(1)\big)\hat{G}^R(1,2) = \delta(1-2)\hat{1}, \tag{3.29a}$$

$$\hat{G}^R(1,2)\big(i\partial_{t_2}\hat{\rho}_3 - \hat{H}(2))\big)^\dagger = \delta(1-2)\hat{1} \tag{3.29b}$$

and similarly for the advanced and Keldysh Green's functions:

$$\big(i\partial_t\hat{\rho}_3 - \hat{H}(1)\big)\hat{G}^A(1,2) = \delta(1-2)\hat{1}, \tag{3.30a}$$

$$\hat{G}^A(1,2)\big(i\partial_{t_2}\hat{\rho}_3 - \hat{H}(2))\big)^\dagger = \delta(1-2)\hat{1} \tag{3.30b}$$

$$\big(i\partial_t\hat{\rho}_3 - \hat{H}(1)\big)\hat{G}^K(1,2) = 0, \tag{3.31a}$$

$$\hat{G}^K(1,2)\big(i\partial_{t_2}\hat{\rho}_3 - \hat{H}(2))\big)^\dagger = 0. \tag{3.31b}$$

Combining these into the 8x8 matrix representation, the eqution of motions are:

$$\big(i\partial_{t_1}\hat{\rho}_3 - \hat{H}(1)\big)\check{G}(1,2) = \delta(1-2)\check{1} \tag{3.32a}$$

$$\check{G}(1,2)\big(i\partial_{t_2}\hat{\rho}_3 - \hat{H}(2)\big)^\dagger = \delta(1-2)\check{1}. \tag{3.32b}$$

Eq. (3.32a) and (3.32b) are the Gor'kov equations [31], which can be combined by appreciating that their right hand sides are equal, and subtracting one from the other gives:

$$\big(i\partial_{t_1}\hat{\rho}_3 - \hat{H}(1)\big)\check{G}(1,2) - \check{G}(1,2)\big(i\partial_{t_2}\hat{\rho}_3 - \hat{H}(2)\big)^\dagger = 0, \tag{3.33}$$

3.6 The quasiclassical approximation

Proceeding, the quasiclassical approximation is applied, which implies integrating over the momentum, effectively selecting the Fermi momentum, $\boldsymbol{p}_F$, as the main realm at which the relevant physics occurs. The reasoning for this comes from appreciating the fact that most of the bodies taking part in the interesting processes have momentum close to $\boldsymbol{p}_F$, bodies with lower momentum are effectively inactive, and above $\boldsymbol{p}_F$ there simply are no bodies to fill the states.

The approximation starts by representing the Gor'kov equations from (3.33)in the Wigner formalism, a process where the fast oscillations of the Green's function is separated from the slowly varying envelope with the relative coordinates:

$$\boldsymbol{r} = \boldsymbol{r}_1 - \boldsymbol{r}_2, \tag{3.34a}$$
$$\boldsymbol{R} = \frac{1}{2}(\boldsymbol{r}_1 + \boldsymbol{r}_2), \tag{3.34b}$$
$$t = t_1 - t_2, \tag{3.34c}$$
$$T = \frac{1}{2} = (t_1 + t_2), \tag{3.34d}$$

resulting in the coordinate transformed Gor'kov equation:

$$\begin{aligned} &i\hbar\big(\partial_{t_1}\check{\rho}_3\check{G}(1,2) + \partial_{t_2}\check{G}(1,2)\check{\rho}_3\big) + \frac{\hbar^2}{2m}\big(\nabla_1^2 - \nabla_2^2\big)\check{G}(1,2) \\ &- i\frac{\hbar}{m}\big[\check{\boldsymbol{A}}(\boldsymbol{r}_1)\cdot\nabla_1\check{G}(1,2) + \nabla_2\check{G}(1,2)\cdot\check{\boldsymbol{A}}(\boldsymbol{r}_2)\big] - \frac{1}{2m}\big[\check{\boldsymbol{A}}^2(\boldsymbol{r}_1)\check{G}(1,2) - \check{G}(1,2)\check{\boldsymbol{A}}(\boldsymbol{r}_2)\big] \\ &- \big[V_{imp}(\boldsymbol{r}_1) - V_{imp}(\boldsymbol{r}_2)\big]\check{G} + \big[\check{\Delta}(\boldsymbol{r}_1)\check{G}(1,2) - \check{G}(1,2)\check{\Delta}(\boldsymbol{r}_2)\big] = 0. \end{aligned} \tag{3.35}$$

Fourier transforming eq. (3.35) by the use of the convolution theorem gives[39][36]:

$$\begin{aligned} \frac{i\hbar}{m}\boldsymbol{p}\cdot\left(\nabla_R\check{\mathcal{G}} - \frac{i}{\hbar^2}\big[\check{\boldsymbol{A}}\overset{\otimes}{,}\check{\mathcal{G}}\big]\right) + \left[\epsilon\check{\rho}_3 - \frac{1}{2m}\check{\boldsymbol{A}}^2 - V_{imp}\check{I}\overset{\otimes}{,}\check{\mathcal{G}}\right] \\ - \frac{i\hbar}{2m}\big\{\boldsymbol{A}\overset{\otimes}{,}\check{\nabla}_R\check{\mathcal{G}}\big\} = 0, \end{aligned} \tag{3.36}$$

where $\otimes$ denotes the convolution of two functions. Omitting terms that are small and introducing the quasiclassical Green's function:

$$\check{g}(\boldsymbol{R}, T, \boldsymbol{p}_F, \epsilon) = \frac{i}{\pi} \int d\xi_p \check{\mathcal{G}}(\boldsymbol{R}, T, \boldsymbol{p}, \epsilon), \tag{3.37}$$

one eventually arrives at the Eilenberger equation:

$$\frac{i\hbar}{m} \boldsymbol{p}_F \cdot \bar{\nabla} \check{g} + \left[\epsilon \check{\rho}_3 - V_{imp} \check{I} - \check{\Delta}, \check{g}\right] = 0. \tag{3.38}$$

3.7 The dirty limit

Accounting for the impurities of the system, and their effect on the electron trajectories, it is assumed that the system contains such a large amount of impurities that the mean free path of the electrons becomes shorter than their coherence length. Consequently, the Green's function is taken to be spherically symmetric. The resulting kinetic equation is called the Usadel equation [36]:

$$\mathcal{D} \bar{\nabla} \left(\check{g}_s \bar{\nabla} \check{g}_s \right) + i \left[\epsilon \check{\rho}_3 - \check{\Delta},\ \check{g}_s \right] = 0, \tag{3.39}$$

where $\mathcal{D} = \frac{v_F^2 \hbar \tau}{3}$ is the diffusion constant.

Chapter 4

The system

The set-up of the system is based on the well-known Josephson junction, first presented by Brian Josephson in 1962 [40]. In such a structure, electrons, in the form of Cooper pairs, can tunnel through the weak link from one superconductor to the other, with the shape[41]:

$$J = J_c \sin\theta, \tag{4.1}$$

θ being the phase difference between the two superconducting wave functions, and J_c denoting the critical current of the system.

The plain SNS-junction has no mechanisms which induces spin-supercurrents, and it has been an aim to find set-ups in which spin-supercurrents are present, and also where spin-polarization occurs. This has been shown to be achievable for systems with conventional superconductors and intrinsically textured ferromagnets [42][43], and in set-ups with layers of several ferromagnets [44]. The challenge with these kinds of systems is the control of the magnetisation direction of the individual ferromagnetic layers and hence the control of the spin-supercurrents. Research has been done on systems mainly implementing normal, non-magnetic materials as the weak link, and how to induce spin-supercurrents in those through the implementation of magnetic insulators[45][9]. These kinds of set-ups present ways to control the spin-supercurrents through the system which are practically much simpler, suggesting the application of an external magnetic field as a way to control the spin-supercurrents. However, it would be even more practical to achieve control through an applied voltage, which has been done for charge-supercurrents [10][11][12]. It offers a more stable application, and the mechanisms are already implemented in semi-conductor technology.

In figure 4.1 an illustration of the system set-up is presented. The ratio between the height of the superconducting reservoirs and the normal metal is small, $L \gg d_s$, to prevent the translational flowing normal current, J_n, induced by the voltage bias, from flowing into the superconducting contacts. The superconducting contacts are assumed to behave as reservoirs, immune to the inverse proximity effect, and it is assumed that the system is at a temperature, T, much lower than the superconducting critical temperature, T_c.

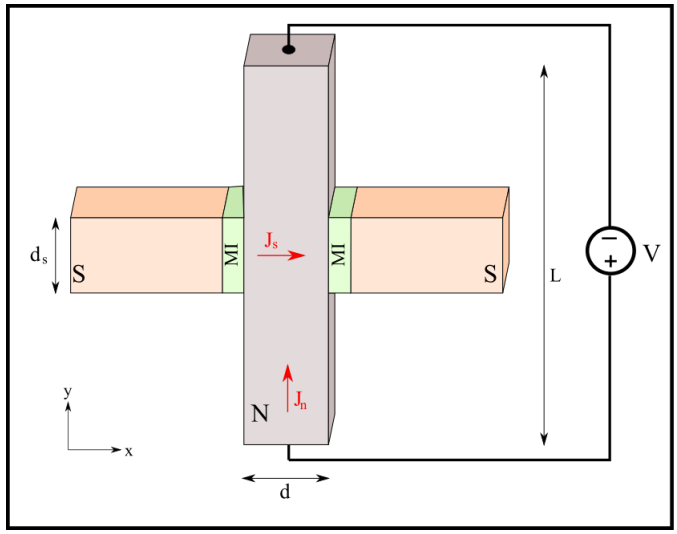

Figure 4.1: Illustration of the system under investigation. S, N and MI stand for Superconductor, Normal metal and Magnetic Insulator respectively.

As mentioned before, the magnetic insulators are responsible for inducing the spin-supercurrent in the system. They polarise the Cooper pairs coming from the superconductors, and offer a way to induce long-range spin-supercurrents in the first harmonic[9]. By contrast, when using layers of two ferromagnetic materials, long-range spin-supercurrents are found, but in the second harmonic [46], which are harder to detect in the lab, and falls short in comparison.

Chapter 5

Solving the Usadel equation

With the Usadel equation established in section 3:

$$\mathcal{D}\nabla(\hat{g}^R\nabla\hat{g}^R) + i\left[\varepsilon\hat{\rho}_3 - \hat{\Delta}, \hat{g}^R\right] = 0, \tag{5.1}$$

solutions for the normal metal and the superconducting reservoirs can be found.

5.1 Solution for the normal metal

For an isolated, bulk normal metal $\Delta = 0$, and the Green's function becomes:

$$\hat{g}^R = \begin{pmatrix} 1 & 0 \\ 0 & -1 \end{pmatrix}, \tag{5.2}$$

whereas in the near proximity of a superconductor, assuming the weak proximity effect, it contains the anomalous, off-diagonal, terms characteristic for systems with Cooper pairs:

$$\hat{g}^R = \begin{pmatrix} 1 & f \\ -\tilde{f} & -1 \end{pmatrix}, \tag{5.3}$$

where f is defined as the 2x2 matrix:

$$f = \begin{pmatrix} f_\uparrow & f_t + f_s \\ f_t - f_s & f_\downarrow \end{pmatrix} \tag{5.4}$$

and the tilde-notation denotes the complex conjugated and energy-inversed counterpart of f, $\tilde{f}(\epsilon) = (f(-\epsilon))^*$ Inserting $\hat{g}^R$ from eq. (5.3) into the Usadel equation one obtains the matrix equation:

$$\begin{pmatrix} -\partial_x f \partial_x \tilde{f} & \partial_x^2 f \\ \partial_x^2 \tilde{f} & -\partial_x \tilde{f} \partial_x f \end{pmatrix} = -\frac{2i\varepsilon}{\mathcal{D}} \begin{pmatrix} 0 & f \\ \tilde{f} & 0 \end{pmatrix} \tag{5.5a}$$

which gives the general solutions for the anomalous Green's function:

$$f_\eta = A_\eta e^{i\kappa x} + B_\eta e^{-i\kappa x} \tag{5.6}$$

where $\kappa = \sqrt{\frac{2i\varepsilon}{\mathcal{D}}}$ and $\eta = \uparrow, \downarrow, s, t$ denoting the type of spin pairing of the Cooper pair: equal spin up or down, singlet and spin zero triplet.

To find the expressions for the coefficients, A_η and B_η, boundary conditions, presented in section 6, are applied. The full solution for the anomalous Green's functions f_η are found and presented in section 9.

5.2 Solution for a bulk BCS superconductor

The Green's function for a bulk superconductor is [36][35]:

$$\hat{g}^R(\varepsilon) = \left[\frac{\mathrm{sgn}(\varepsilon)}{\sqrt{\varepsilon^2 - |\Delta|^2}} \theta(\varepsilon^2 - \Delta^2) - \frac{i}{\sqrt{|\Delta|^2 - \varepsilon^2}} \theta(\Delta^2 - \varepsilon^2) \right] \left(\varepsilon \hat{\rho}_3 + \hat{\Delta} \right). \quad (5.7)$$

The solution for the superconductive regions are included in the calculations throught the boundary conditions, presented in section 6.

Chapter 6

Boundary conditions

The abrupt nature of the boundaries in the system makes it necessary to introduce boundary conditions for isotropic Greens functions (BCIGF) to describe the transition from the superconductor, across the magnetic insulator and into the normal material, and henceforth the mirrored path into the superconductor on the other side of the junction. The quasiclassical and isotropic approximations applied in the Usadel equations are invalid near the interfaces of the system which means that the boundary conditions are not derived in the quasiclassical limit. Rather, they are a combination and matching of the microscopic descriptions of four model regions near the interface: the diffusive, isotropic, ballistic and scattering region. See figure 6.1 for a visualisation. By asymptotic matching of the wavefunctions across the boundaries between these regions, the result is the Nazarov boundary conditions [47], valid for arbitrary barrier transparency, T_n. Assuming low transparency, $T_n \gg 1$, they can be simplified into the Kupriyanov-Lukichev(KL) boundary conditions [48], which suits the system at hand. To account for the spin active insulators, additional terms are added to the KL-conditions [49], and the following equations are obtained:

$$2d\zeta_L\big(\check{g}_j\partial_x\check{g}_j\big) = \big[\check{g}_i,\check{g}_j\big] + G_{MR}\big[\check{g}_i,\{\hat{A},\check{g}_j\}\big] + iG_\phi^L\big[\check{g}_i,\hat{A}\big], \quad x=0 \tag{6.1a}$$

$$2d\zeta_R\big(\check{g}_j\partial_x\check{g}_j\big) = \big[\check{g}_j,\check{g}_k\big] - G_{MR}\big[\check{g}_j,\{\hat{A},\check{g}_k\}\big] - iG_\phi^R\big[\check{g}_j,\hat{A}\big], \quad x=d \tag{6.1b}$$

Where d is the length of the normal metal, $\zeta_{L(R)} = R_B/R_{L(R)}$: R_B being the resistance of the normal metal and $R_{L(R)}$ is the bulk resistance of the left(right) superconductor. The indices *i,j,k* represent the left side superconductor, the normal metal and the right side superconductor respectively. $G_\phi^{L(R)}$ is the spin mixing term, defined as $G_\phi^{L(R)} = -\sum_n d\phi_n^{L(R)}/\sum_n T_n$. T_n is the transmission probability and $d\phi_n^{L(R)}$ is the spin-mixing angle. It introduces the spin-dependent phase shift at the left(right) side of the the junction. G_{MR} includes magnetoresistance at the boundary contributing as a damper on the superconducting proximity effect. It has been verified that a spin-supercurrent is present even when G_{MR} is included [9], but is neglected for simplicity in the forthcoming text. $\hat{A}$ is called the boundary matrix, containing the magnetisation direction $\boldsymbol{m}$, and the Pauli vector $\hat{\boldsymbol{\sigma}} = (\hat{\sigma}_1 + \hat{\sigma}_2 + \hat{\sigma}_3)$:

$$\hat{A} = \begin{pmatrix} \boldsymbol{m}\cdot\hat{\boldsymbol{\sigma}} & 0 \\ 0 & \boldsymbol{m}\cdot\hat{\boldsymbol{\sigma}}^* \end{pmatrix} \tag{6.2}$$

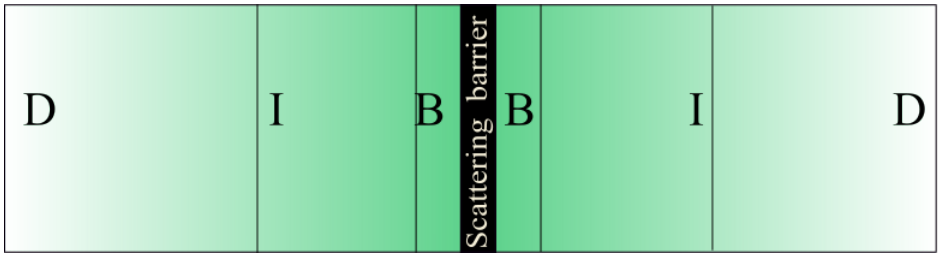

Figure 6.1: Visualisation of the division into different regions near the interface. D, I B stand for diffusive, isotropic and ballistic regions respectively.

As previously, the conditions in eq. (6.1) can be expressed solely in terms of the retarded Green's function, and dropping the magnetoresistance term G_{MR}, the conditions read:

$$2d\zeta_L\left(\hat{g}_j^R\partial_x\hat{g}_j^R\right) = \left[\hat{g}_i^R,\hat{g}_j^R\right] + iG_\phi^L\left[\hat{g}_i^R,\hat{A}\right], \qquad x=0 \tag{6.3a}$$

$$2d\zeta_R\left(\hat{g}_j^R\partial_x\hat{g}_j^R\right) = \left[\hat{g}_j^R,\hat{g}_k^R\right] - iG_\phi^R\left[\hat{g}_j^R,\hat{A}\right], \qquad x=d \tag{6.3b}$$

reducing the size of the matrices, making the equations less cumbersome to work with.

Chapter 7

The distribution function

The distribution function for the superconducting hybrid system is important as it gives the occupation of states. With the density of states given by the Green's functions, the equilibrium distribution function for the Cooper pairs falls out of the normalisation condition of the 8x8 Keldysh Green's function $(\check{G})^2 = \check{1}$:

$$\hat{G}^R\hat{G}^K + \hat{G}^K\hat{G}^A = 0 \tag{7.1}$$

which gives the expression for the upper right Keldysh component:

$$\hat{G}^K = \hat{G}^R\hat{h} - \hat{h}\hat{G}^A \tag{7.2}$$

where $\hat{h}$ is the distribution matrix. Following the lines of Ref. [50], $\hat{h}$ takes the diagonal form:

$$\hat{h} = \begin{pmatrix} \tanh(\beta(\epsilon + eV)) & 0 \\ 0 & \tanh(\beta(\epsilon - eV)) \end{pmatrix} \tag{7.3}$$

The non-equilibrium distribution function for the system is given by the stationary diffusive Boltzmann equation[51]:

$$\mathcal{D}\partial_y^2\mathcal{F} + C(\mathcal{F}) = 0 \tag{7.4}$$

where $\mathcal{D}$ is the familiar electron diffusion constant and $C(\mathcal{F})$ is a collision integral accounting for inelastic scattering of the electrons in N. It is set to zero as the length of the normal metal, d, is shorter than the inelastic scattering length of the electrons. The solution of the diffusion equation is then:

$$\mathcal{F}(\epsilon, y) = \left(\frac{1}{2} - \frac{y}{L}\right)\mathcal{F}^{eq}\Big(\epsilon + U\Big) + \left(\frac{1}{2} + \frac{y}{L}\right)\mathcal{F}^{eq}\Big(\epsilon + U\Big) \tag{7.5}$$

Applying a voltage bias in this order shifts the quasi-particle's energies by $\pm\frac{eV}{2}$, so that $\mathcal{F}_{L/2}(\epsilon, \frac{L}{2}) = \mathcal{F}_0(\epsilon - \frac{eV}{2})$ and $\mathcal{F}_{-L/2}(\epsilon, -\frac{L}{2}) = \mathcal{F}_0(\epsilon + \frac{eV}{2})$, where $\mathcal{F}_0$ is the Fermi-Dirac distribution:

$$\mathcal{F}_0 = \frac{1}{e^{\beta\epsilon} + 1} \tag{7.6}$$

The non-equilibrium distribution function has a step-function form with respect to energy, with the familiar Fermi-Dirac shape at the edges of the y-length, and

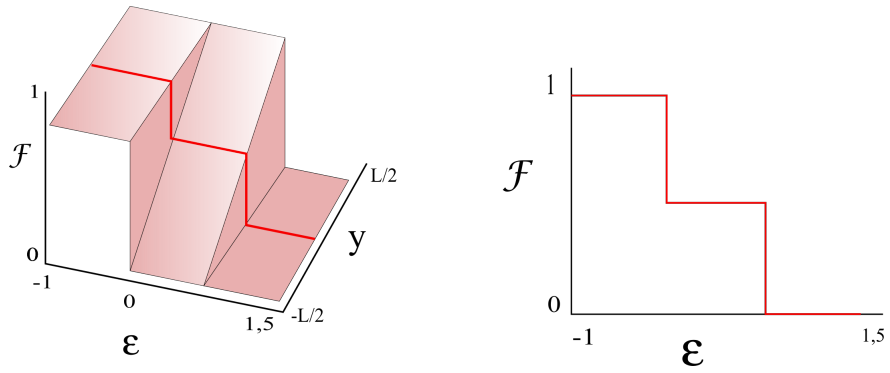

Figure 7.1: Schematic of the distribution function in the normal metal when a voltage bias is applied.

goes over to a double-step function along the y-length, see figure 7.1.

The full non-equilibrium quasiparticle distribution function reads:

$$\mathcal{F}(\epsilon, y) = \frac{1}{2}\left(\left[\frac{1}{e^{\beta(\epsilon+\frac{eV}{2})}+1}\right] + \left[\frac{1}{e^{\beta(\epsilon-\frac{eV}{2})}+1}\right]\right), \tag{7.7}$$

where $\beta = (k_B T)^{-1}$.

Following the set-up in reference [10], the distribution function is implemented in the form $(1 - 2\mathcal{F}(\varepsilon, y))$.

Chapter 8

Physical observables - the current

Physical observables are of great interest as they are measurable in the lab. Presented in this chapter is the derivation of the charge and spin currents of the system.
The quasiclassical charge and spin currents are defined as:

$$I_Q = I_{Q,0} \int_{-\infty}^{\infty} d\epsilon \ \ Tr\Big\{ \hat{\rho}_3 (\check{g}\partial_x \check{g})^K \Big\}, \tag{8.1}$$

$$I_s^\nu = I_{s,0} \int_{-\infty}^{\infty} d\epsilon \ \ Tr\Big\{ \hat{\rho}_3 \hat{\tau}_\nu (\check{g}\partial_x \check{g})^K \Big\}. \tag{8.2}$$

$I_{Q,0} = \frac{N_0 e D A}{4}$, $I_{s,0} = \frac{N_0 \hbar D A}{8}$, where N_0 is the density of states at the normal-state Fermi-level, e is the electron charge, $\hbar$ is the reduced Planck constant, A is the interface contact area and $\nu = x, y, z$. The full derivation of the expression in (8.1) can be found in Appendix B. These expressions can be written in terms of the retarded 4x4 matrix Greens function:

$$I_Q = I_{Q,0} \int_{-\infty}^{\infty} d\epsilon \ \ (1 - 2\mathcal{F}(\epsilon, y)) \mathrm{Tr} \Big\{ \hat{\rho}_3 \big(\hat{g}^R \partial_x \hat{g}^R \big) \Big\}, \tag{8.3}$$

$$I_s^\nu = I_{s,0} \int_{-\infty}^{\infty} d\epsilon \ \ (1 - 2\mathcal{F}(\epsilon, y)) \mathrm{Tr} \Big\{ \hat{\rho}_3 \hat{\tau}_\nu \big(\hat{g}^R \partial_x \hat{g}^R \big) \Big\}, \tag{8.4}$$

where the distribution function falls out from the normalisation condition discussed in section 7. Furthermore, the expressions can be simplified to:

$$I_Q = I_{Q,0} \int_{0}^{\infty} d\epsilon \ \ (1 - 2\mathcal{F}(\epsilon, y)) 4\mathrm{Re}\big\{ f_Q(\epsilon) \big\} \tag{8.5}$$

by using the definition: $\tilde{f} = f^*(-\epsilon)$ and performing the traces. Due to the structure of the Pauli matrices, the y-component of the spin-current differs slightly from the x and z-components:

$$I_s^{x,z} = I_{s,0} \int_{0}^{\infty} d\epsilon \ \ (1 - 2\mathcal{F}(\epsilon, y)) 4\mathrm{Re}\big\{ f_s^{x,z}(\epsilon) \big\} \tag{8.6a}$$

$$I_s^{y} = I_{s,0} \int_{0}^{\infty} d\epsilon \ \ (1 - 2\mathcal{F}(\epsilon, y)) 4\mathrm{Im}\big\{ f_s^{y}(\epsilon) \big\} \tag{8.6b}$$

In section 9, explicit expression for $f_Q(\epsilon)$ and $f_s^\nu(\epsilon)$, and hence the currents are presented.

Chapter 9

Analytical work

9.1 The general form

To find the coefficients, $\hat{A}, \hat{B}, \tilde{A}$ and $\tilde{B}$ the boundary conditions defined in eq. (6.1) are applied.

The junction to the left is considered first, located at $x = 0$. Here, the superconducting Green's function is denoted: $\hat{g}_1^R$, and the normal metal Green's function denoted: $\hat{g}_2^R$. It is noted now that the hat-notation denotes a 4x4 matrix, and the elements within that matrix is left with no implicit 2x2 notation, due to brevity. The lhs. of eq. (6.3a) can be written out:

$$\hat{g}_2^R \partial_x \hat{g}_2^R = \begin{pmatrix} -f\partial_x \tilde{f} & \partial_x f \\ \partial_x \tilde{f} & -\tilde{f}\partial_x f. \end{pmatrix} \tag{9.1}$$

The first term of the rhs. of eq(6.3a) becomes:

$$[\hat{g}_1^R, \hat{g}_2^R] = \begin{pmatrix} -\Delta\tilde{f} + f\Delta & \varepsilon f + f\varepsilon - 2\Delta \\ \varepsilon\tilde{f} + \tilde{f}\bar{\varepsilon} - 2\Delta^* & -\Delta^* f + \tilde{f}\Delta, \end{pmatrix} \tag{9.2}$$

and the last term:

$$iG_\phi^L[\hat{g}_2^R, \hat{A}] = iG_\phi^L \begin{pmatrix} 0 & f(\boldsymbol{m_L}\cdot\boldsymbol{\sigma^*}) - (\boldsymbol{m_L}\cdot\boldsymbol{\sigma})f \\ -\tilde{f}(\boldsymbol{m_L}\cdot\boldsymbol{\sigma}) + (\boldsymbol{m_L}\cdot\boldsymbol{\sigma^*})\tilde{f} & 0 \end{pmatrix}. \tag{9.3}$$

Appreciating that the anomalous Green's functions, f and $\tilde{f}$ are small, $f, \tilde{f} \ll 1$, in the weak proximity regime, the off-diagonal terms in equation (9.2) can be simplified to:

$$\varepsilon f + f\varepsilon - 2\Delta \simeq -2\Delta \tag{9.4}$$

Which leaves the following equation for f:

$$2d\zeta_L \partial_x f = -2\Delta + iG_\phi^L \Big\{ f(\boldsymbol{m_L}\cdot\boldsymbol{\sigma^*}) - (\boldsymbol{m_L}\cdot\boldsymbol{\sigma})f \Big\}, \tag{9.5}$$

compacted with $\boldsymbol{M} = f(\boldsymbol{m_L}\cdot\boldsymbol{\sigma^*}) - (\boldsymbol{m_L}\cdot\boldsymbol{\sigma})f$ into:

$$2d\zeta_L \partial_x f = -2\Delta + iG_\phi^L \boldsymbol{M}. \tag{9.6}$$

where Δ is the 2x2 matrix:

$$\Delta = \begin{pmatrix} 0 & |\Delta_0| e^{i\theta_L} \\ |\Delta_0| e^{-i\theta_L} & 0 \end{pmatrix}. \tag{9.7}$$

Writing out the spin-dependent terms:

$$iG_\phi^L \boldsymbol{M} = iG_\phi^L \begin{pmatrix} f_\uparrow & f_t + f_s \\ f_t - f_s & f_\downarrow \end{pmatrix} \begin{pmatrix} m_z & m_x + im_y \\ m_x - im_y & -m_z \end{pmatrix} - \tag{9.8a}$$

$$\begin{pmatrix} m_z & m_x - im_y \\ m_x + im_y & -m_z \end{pmatrix} \begin{pmatrix} f_\uparrow & f_t + f_s \\ f_t - f_s & f_\downarrow \end{pmatrix}, \tag{9.8b}$$

results in the following equations:

$$iG_\phi^L \boldsymbol{M}_{11} = 2iG_\phi^L f_s (m_x - im_y), \tag{9.9a}$$

$$iG_\phi^L \boldsymbol{M}_{12} = iG_\phi^L (m_x + im_y) f_\uparrow - 2(f_t + f_s) m_z - (m_x - im_y) f_\downarrow, \tag{9.9b}$$

$$iG_\phi^L \boldsymbol{M}_{21} = -iG_\phi^L f_\uparrow (m_x + im_y) + 2(f_t - f_s) + f_\downarrow (m_x - im_y), \tag{9.9c}$$

$$iG_\phi^L \boldsymbol{M}_{21} = -iG_\phi^L 2 f_s (m_x + im_y). \tag{9.9d}$$

Following the same approach for the rhs. of the system, at x=d, results in eight

equations:

$$d\zeta_L \partial_x f_\uparrow \Big|_{x=0} = iG_\phi^L f_s (m_x^L - im_y^L), \tag{9.10a}$$

$$d\zeta_L \partial_x f_\downarrow \Big|_{x=0} = -iG_\phi^L f_s (m_x^L + im_y^L), \tag{9.10b}$$

$$d\zeta_L \partial_x f_t \Big|_{x=0} = -iG_\phi^L f_s m_z^L, \tag{9.10c}$$

$$d\zeta_L \partial_x f_s \Big|_{x=0} = -|\Delta_0| e^{i\theta_L} - \frac{i}{2} G_\phi^L \Big\{ (m_x^L + im_y^L) f_\uparrow - (m_x^L - im_y^L) f_\downarrow - 2m_z^L f_t \Big\}, \tag{9.10d}$$

$$d\zeta_R \partial_x f_\uparrow \Big|_{x=d} = -iG_\phi^R f_s (m_x^R - im_y^R), \tag{9.10e}$$

$$d\zeta_R \partial_x f_\downarrow \Big|_{x=d} = iG_\phi^R f_s (m_x^R + im_y^R), \tag{9.10f}$$

$$d\zeta_R \partial_x f_t \Big|_{x=d} = iG_\phi^R f_s m_z^R, \tag{9.10g}$$

$$d\zeta_R \partial_x f_s \Big|_{x=d} = |\Delta_0| e^{i\theta_R} + \frac{i}{2} G_\phi^R \Big\{ (m_x^R + im_y^R) f_\uparrow - (m_x^R - im_y^R) f_\downarrow - 2m_z^R f_t \Big\}, \tag{9.10h}$$

Solving this system of equations gives expressions for the eight coefficients. Inserted into the current expressions from (8.1) and (8.2) this gives:

$$I_Q = I_0 \sin\theta \int_0^\infty d\varepsilon \big(1 - 2\mathcal{F}(\varepsilon, y)\big) 4\mathrm{Re}\Bigg(4i\kappa \sin(\kappa d) \Omega^{-1} \big\{ G_\phi^L G_\phi^R (\boldsymbol{m}^L \cdot \boldsymbol{m}^R) + \zeta_L \zeta_R d^2 \kappa^2 \big\} \Bigg), \tag{9.11}$$

$$\begin{aligned} |I_s| = I_0 \int_0^\infty d\varepsilon \, \big(1 - 2\mathcal{F}(\varepsilon, y)\big) 16 i\kappa G_\phi^L G_\phi^R S^2 \Delta^2 \sin(\kappa d) |\boldsymbol{m}^L \times \boldsymbol{m}^R| \Omega^{-2} \Bigg(\cos\theta \big([h_L (G_\phi^L)^2 \\ + \kappa^2 d^2 \zeta_L][h_R (G_\phi^R)^2 + \kappa^2 d^2 \zeta_R] \cos^2(\kappa d) + [w G_\phi^L G_\phi^R + \kappa^2 d^2 \zeta_L \zeta_R]^2 \big) \\ + \big([h_L (G_\phi^L)^2 + h_R (G_\phi^R)^2 + \kappa^2 d^2 (\zeta_L^2 + \zeta_R^2)][w G_\phi^L G_\phi^R + \kappa^2 d^2 \zeta_L \zeta_R] \big) \cos(\kappa d) \Bigg), \end{aligned} \tag{9.12}$$

where $|I_s|$ is the absolute value of the spin current: $\sqrt{(I_s^x)^2 + (I_s^y)^2 + (I_s^z)^2}$, and Ω denotes the denominator:

$$\Omega = \big[h_L (G_\phi^L)^2 + \kappa^2 d^2 \zeta_L^2 \big] \big[h_R (G_\phi^R)^2 + \kappa^2 d^2 \zeta_R^2 \big] \cos^2(\kappa d) - \big[w G_\phi^L G_\phi^R + \kappa^2 d^2 \zeta_L \zeta_R \big]. \tag{9.13}$$

Also, the parameters h_L, h_R and w are introduced to simplify the expressions:

$$h_L = (m_L^z)^2 - (m_L^x)^2 - (m_L^y)^2 \tag{9.14a}$$
$$h_R = (m_R^z)^2 - (m_R^x)^2 - (m_R^y)^2 \tag{9.14b}$$
$$w \ = m_L^x m_R^x + m_L^y m_R^y - m_L^z m_R^z. \tag{9.14c}$$

The magnetisation dependence of the currents I_Q and I_s comes through as depending on the relative angles between the left and right insulator, and therefore the angles in the right insulator can be locked without any loss of generality. The choice of magnetisation angle is based on the choice made in ref. [9]: $\boldsymbol{m}^R = (0, 0, 1)$, to make comparisons to their analytical results simpler. With this convention in place, the expressions for the supercurrents are:

$$I_Q = I_0 \sin\theta \int_0^\infty d\varepsilon \, \big(1 - 2\mathcal{F}(\varepsilon, y)\big) 4\mathrm{Re}\bigg(4i\kappa \, \Sigma^{-1} \sin(\kappa d) \big\{ G_\phi^L G_\phi^R \cos\alpha + \zeta_L \zeta_R d^2 \kappa^2 \big\} \bigg), \tag{9.15a}$$

$$I_s^x = I_0 \, \sin\phi \sin\alpha \, G_\phi^L G_\phi^R \int_0^\infty d\varepsilon \, \big(1 - 2\mathcal{F}(\varepsilon, y)\big) 4\mathrm{Re}\bigg(\Sigma^{-2} i\kappa \sin(\kappa d) S^2 \Delta^2 \big[\lambda_1 + \lambda_2 \cos\theta\big] \bigg), \tag{9.15b}$$

$$I_s^y = -\frac{\cos\phi}{\sin\phi} \, I_s^x, \tag{9.15c}$$

$$I_s^z = 0. \tag{9.15d}$$

The coefficients Σ, λ_1 and λ_2 are defined as:

$$\begin{aligned}
\Sigma &= \big[\kappa^2 d^2 \zeta_L^2 + 2(G_\phi^L)^2 \cos^2\alpha - (G_\phi^L)^2\big] \big[\kappa^2 d^2 \zeta_R^2 + (G_\phi^R)^2\big] \cos^2(\kappa d) \\
&\quad - \big[\kappa^2 d^2 \zeta_L \zeta_R - G_\phi^L G_\phi^R \cos\alpha\big]^2 \\
\lambda_1 &= \big[2(G_\phi^L)^2 \cos^2\alpha - (G_\phi^L)^2 + \kappa^2 d^2 (\zeta_L + \zeta_R) + (G_\phi^R)^2\big] \big[\kappa^2 d^2 \zeta_L \zeta_R + G_\phi^L G_\phi^R \cos\alpha\big]^2 \\
\lambda_2 &= \big[\kappa^2 d^2 \zeta_L^2 + 2(G_\phi^L)^2 \cos^2\alpha - (G_\phi^L)^2\big] \big[\kappa^2 d^2 \zeta_R^2 + (G_\phi^R)^2\big] \cos^2(\kappa d) \\
&\quad + \big[\kappa^2 d^2 \zeta_L \zeta_R - G_\phi^L G_\phi^R \cos\alpha\big]^2
\end{aligned} \tag{9.16}$$

The charge current is fully dependent on the superconducting phase difference, θ , whereas the spin currents is partially dependent on it. This means there exists a spin supercurrent, even when the Josephson current goes to zero for $\theta = 0$. This means that a spin current in the absence of a charge current is achievable, first reported by Gomperud and Linder in 2015[9].

The magnetisation dependence of the spin currents is manifested in the cross product between the right and left magnetic orientation, and with $\boldsymbol{m}_R = (0, 0, 1)$,

it is easy to see that $I_s^z = 0$. Furthermore, the relation between I_s^x and I_s^y becomes quite simple, see eq. (9.15c).

Chapter 10

Numerical results

The numerically obtained results are presented in this section. The approach has been to partially solve the Usadel equation analytically, obtaining a set of linear equations, and solve these numerically. First, some known results has been reproduced and are presented in section 10.1 and 10.2. In section 10.3 the new, non-equilibrium results are presented, first with respect to the superconducting phase difference, θ in subsection 10.3.1, thereafter with respect to the misalignment angle, α in subsection 10.3.2.

10.1 SNS solution

To verify that the numerical results are accountable, special cases already accepted in the literature is reproduced. In figure 10.1, the well known sine shape of the Josephson current is shown. Here, the magnetic insulators are excluded and no voltage bias is applied.

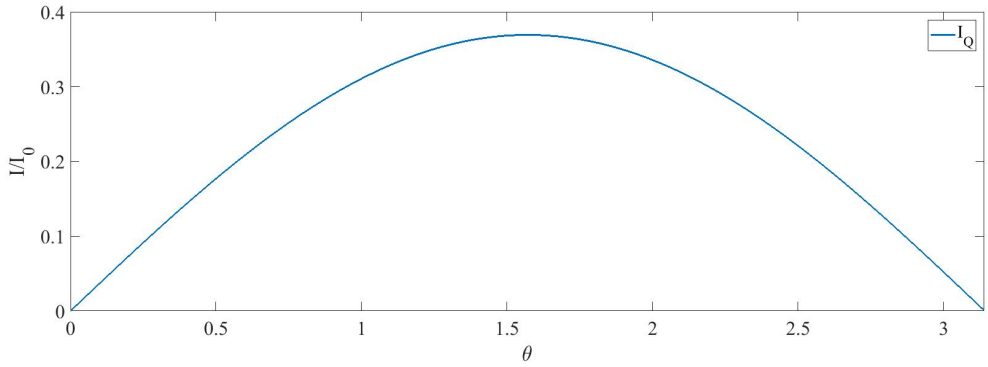

Figure 10.1: Charge-supercurrent as a function of the superconducting phase difference θ. $G_\phi = 0$, $V = 0$. $T/T_c = 0.02$, $d = 20\text{nm}$, $\zeta = 5$ and $\xi_s = 30\text{nm}$.

10.2 Including the magnetic insulators

When the magnetic insulators are included, the spin-supercurrents appear, which is shown in figure 10.2. The sine shape of the charge current is present, and so is the partial $\cos\theta$ form of the spin-supercurrents, confirming the equations in (9.15). It demonstrates the fact that a spin-supercurrent exist when $\theta = 0$, as reported in reference [9]. I_z is zero due to the magnetisation orientation chosen for the magnetic insulator on the right hand side of the junction, as discussed in chapter 9.

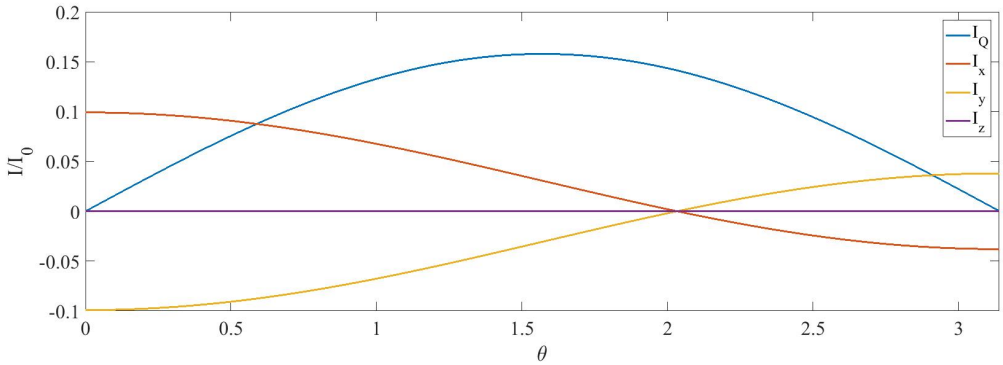

Figure 10.2: Charge and spin current as a function of the superconducting phase difference θ. $G_\phi = 0$, $\alpha = \pi/3$, $\phi = \pi/4$ $T/T_c = 0.02$, $d = 20$ nm, $\zeta = 5$, and $\xi_s = 30$nm.

10.3 Applying a voltage bias

By turning on the voltage across the normal metal, the distribution function is driven out of equilibrium, and it will be shown that the supercurrents are altered. In figure 10.3 the supercurrents are presented as a function of V, and it is demonstrated that both the spin and charge-supercurrents undergoes the $0 - \pi$ transition, but for different values of V. The reason for this is the difference in magnitude of the charge and spin-supercurrents, dependent on their spectral properties, which are different for the charge and spin-supercurrents. The tuning effect controlled by the voltage is implemented through the distribution function, which is the same for both the charge and the spin-supercurrent, as can be seen in their analytical expressions in (9.15). Therefore, I_x and I_y die off faster than I_Q.

The shape of the supercurrents (referring to the I_Q when comparing to reference [10]) vs. V presented here has a peak at low voltages before it decreases and eventually changes sign, which is not present in the results in reference [10]. This can be explained by the fact that the system used in reference [10] is not modelled in the weak proximity limit, which the system investigated in this thesis is. The assumption of weak proximity, meaning that the anomalous Green's function is a lot smaller than 1, $f \ll 1$, does not hold for small energies, which transfers into the small-voltage regime. For high voltages the supercurrents expectedly vanish, as the distribution function goes towards 1/2 and the term $(1 - 2\mathcal{F}(\varepsilon, y))$ goes to zero.

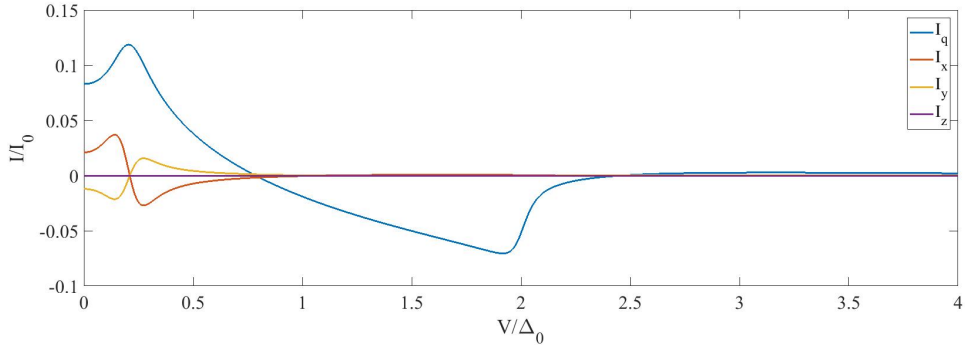

Figure 10.3: The supercurrents as a function of V. $G_\phi = 3$, $\phi = \pi/3$, $\alpha = \pi/2$, $\theta = \pi/2$, $T/T_c = 0.02$, $\zeta = 5$, $\xi_s = 30$nm and $d = 60$nm.

In figure 10.4, it is demonstrated that a change in the normal-metal length, d, increases the voltage needed to achieve the $0 - \pi$ transition. The plot also reveals how the magnitude of the supercurrents increase with shorter lengths of the normal metal. This is a result of the spatial dependence of the superconducting order parameters of the two superconductors in the system. The overlap between the two decreases with increasing d.

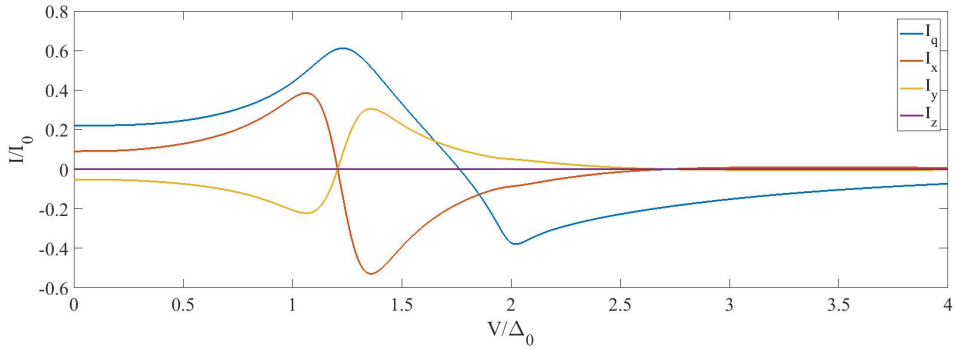

Figure 10.4: The supercurrents as a function of V. $G_\phi = 3$, $\phi = \pi/3$, $\alpha = \pi/2$, $\theta = \pi/2$, $T/T_c = 0.02$, $\zeta = 5$, $\xi_s = 30$nm and $d = 20$nm.

10.3.1 The θ-dependence

In figures 10.5-10.8, the θ-dependence of the supercurrents is shown as a function of V.

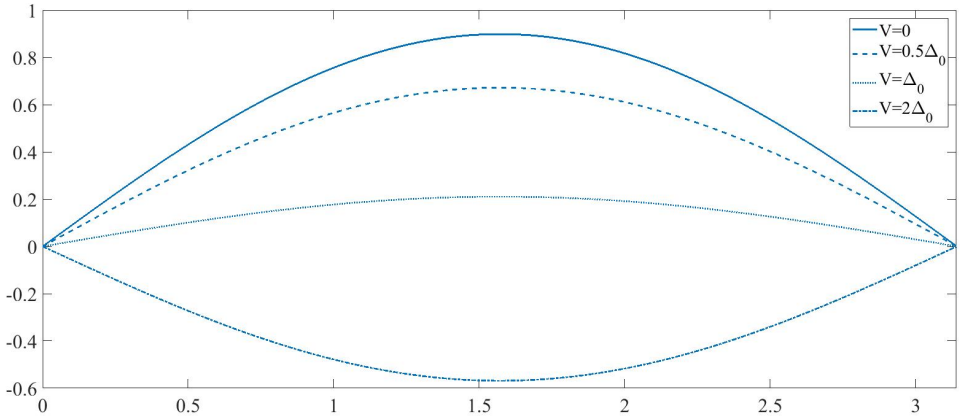

Figure 10.5: Charge-supercurrent as a function of the superconducting phase difference θ, for various values of control voltage. $G_\phi = 0.5$, $d = 20$nm, $\xi_s = 30$nm, $\zeta = 5$, $T/T_c = 0.02$, $\alpha = \pi/3$, $\phi = \pi/4$.

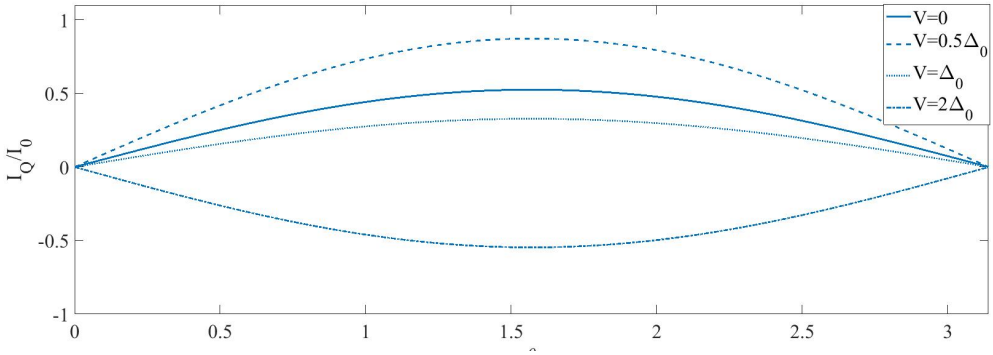

Figure 10.6: Charge-supercurrent as a function of θ, for various values of control voltage. $G_\phi = 1.1$, $d = 20$nm, $\xi_s = 30$nm, $\zeta = 5$, $T/T_c = 0.02$, $\alpha = \pi/3$, $\phi = \pi/4$.

The charge-supercurrent transitions to a π-state with increasing V, whereas the spin-supercurrents go to zero. It is interesting to note that I_y starts off in the π-state due to the difference in ϕ-dependence of I_x and I_y, which goes as $\sin\phi$ and $\cos\phi$ respectively.

Figure 10.5-10.8 presents the supercurrents as functions of θ for $G_\phi = 0.5$ in figure 10.5 and 10.7, and for $G_\phi = 1.1$ in figure 10.6 and 10.8. It shows how an increase in G_ϕ increases the magnitude of the spin-supercurrents, the spin-supercurrents having a total dependence on G_ϕ, and the charge-supercurrent having a partial dependence on G_ϕ. However, for $V < 1/2\ \Delta_0$, this G_ϕ-dependence does not hold.

The reason being that the supercurrents experience a small increase between the voltage interval $0- \sim 1/2\ \Delta_0$. This is the reason the $V = 0$-legend in figure 10.5 and 10.6 does not exhibit this G_ϕ-feature.

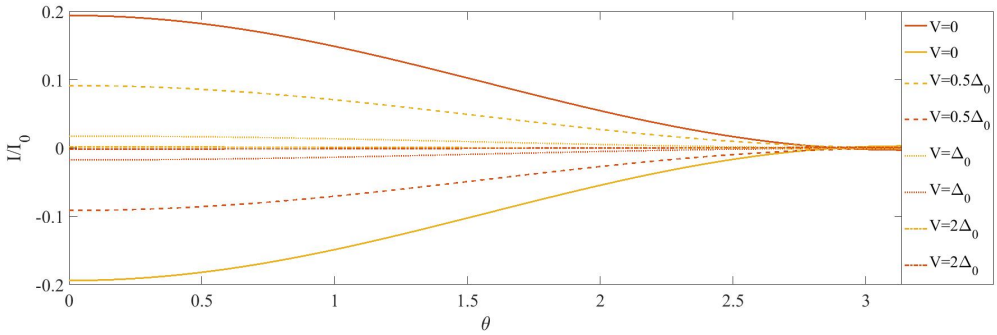

Figure 10.7: I_x(red) and I_y(yellow) as a function of θ, for various values of V. $G_\phi = 0.5$, $d = 20$nm, $\xi_s = 30$nm, $\zeta = 5$, $T/T_c = 0.02$, $\alpha = \pi/3$, $\phi = \pi/4$.

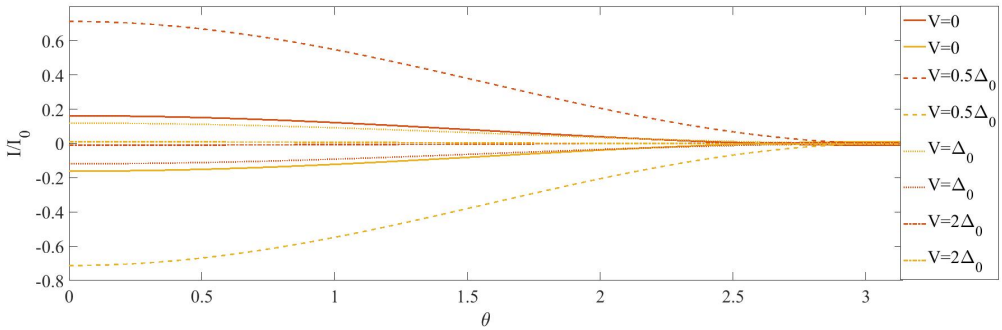

Figure 10.8: I_x(red) and I_y(yellow) as a function of θ, for various values of V. $G_\phi = 1.1$, $d = 20$nm, $\xi_s = 30$nm, $\zeta = 5$, $T/T_c = 0.02$, $\alpha = \pi/3$, $\phi = \pi/4$.

To give a wholesome picture of the V and θ-dependence, surface plots of the supercurrents as functions of V and θ are presented below. Figures 10.9 and 10.10 I_Q is presented as a function of V and θ. G_ϕ is set to 1.5, and comparing to the line plots 10.3 and 10.4, it is confirmed again that an increase in G_ϕ increases the voltage needed to transition to a π-junction.

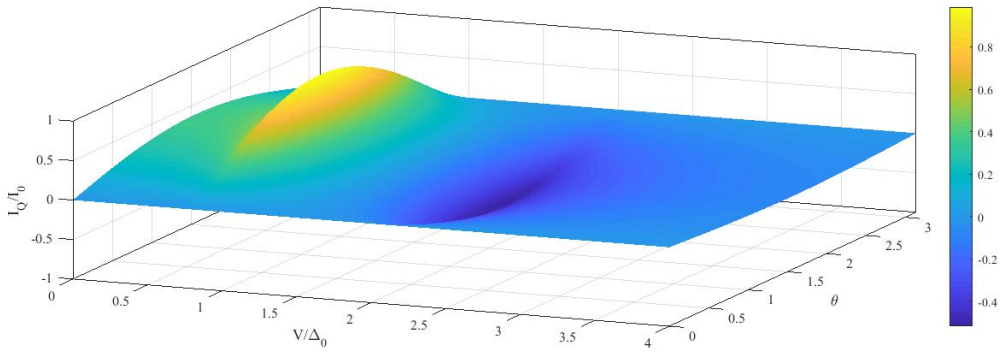

Figure 10.9: I_Q as a function of θ and V. $G_\phi = 1.5$, $T_c/T = 0.02$, $d = 20$nm, $\xi_s = 30$nm, $\zeta = 5$, $\phi = \pi/3$ and $\alpha = \pi/4$.

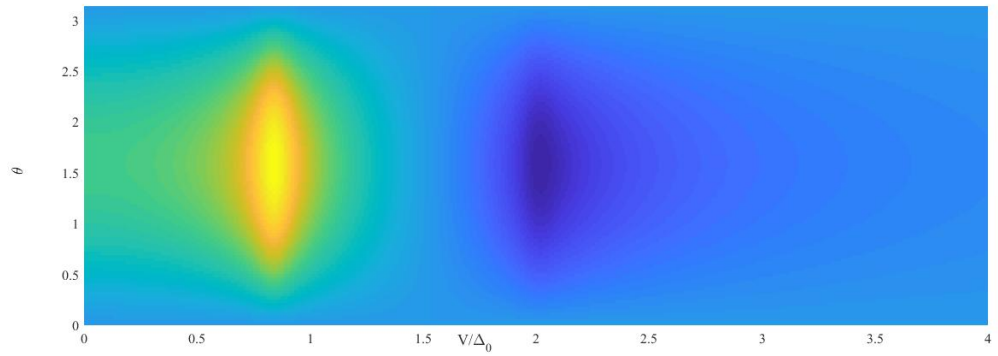

Figure 10.10: I_Q in the plane of V and θ. $G_\phi = 1.5$, $T_c/T = 0.02$, $d = 20$nm, $\xi_s = 30$nm, $\phi = \pi/3$ and $\alpha = \pi/4$.

In figures 10.11 and 10.12, I_x is presented as a function of V and θ. $d = 5$nm and $\phi = \pi/4$. One could assume that the transition value would increase significantly, as seen in figure 10.4 by the decrease of d by 55nm, but due to the decrease of ϕ, the transition value remains the same at $V \sim 0.8\Delta_0$.

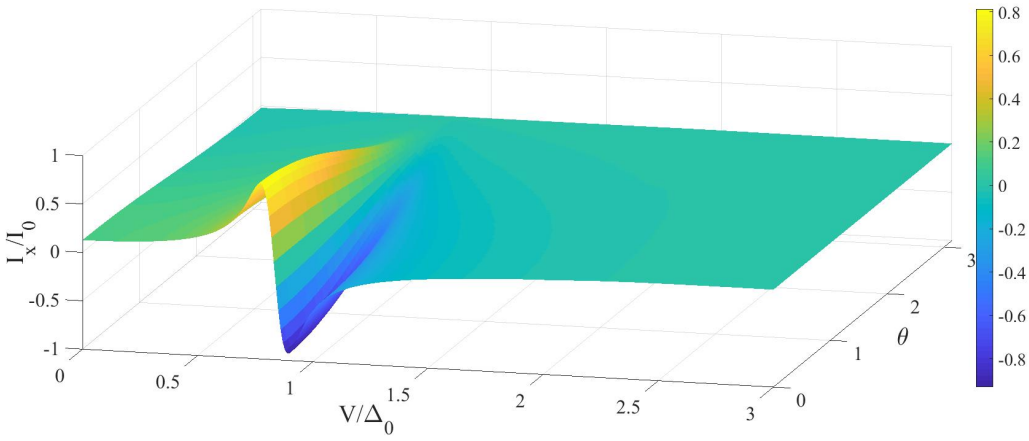

Figure 10.11: I_x as a function of θ and V. $G_\phi = 3$, $\zeta = 2$, $T_c/T = 0.02$, $\phi = \pi/4$, $\alpha = \pi/2$, $\xi_s = 30$nm and $d = 5$nm.

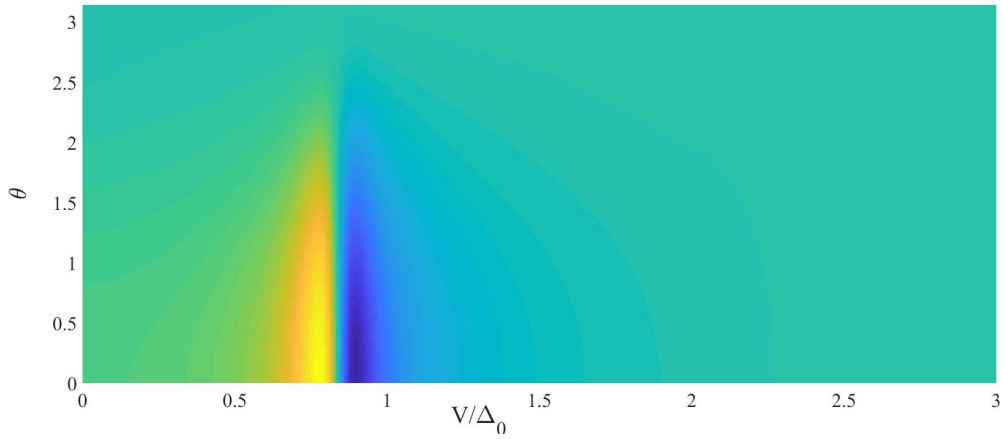

Figure 10.12: I_x in the plane of control voltage V and superconducting phase difference θ.

I_y is presented as a function of V and θ in figures 10.13 and 10.14. As expected, it is similar to I_x in shape, but depicting the opposite sign due to its ϕ-dependence. It undergoes a decrese into negative values before it abruptly increases into a peak of ~ 0.5, and then an exponential decline to zero thereafter.

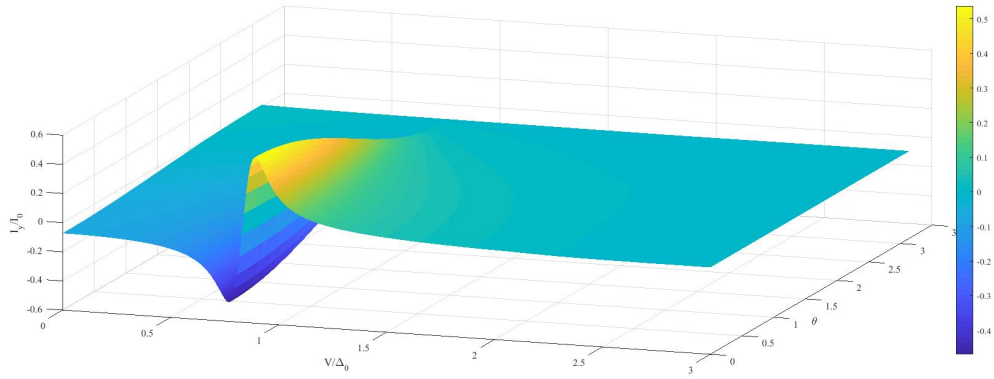

Figure 10.13: I_y as a function of θ V. $G_\phi = 3$, $\zeta = 2$, $T_c/T = 0.02$, $\phi = \pi/4$, $\alpha = \pi/2$, $\xi_s = 30$nm and $d = 5$nm.

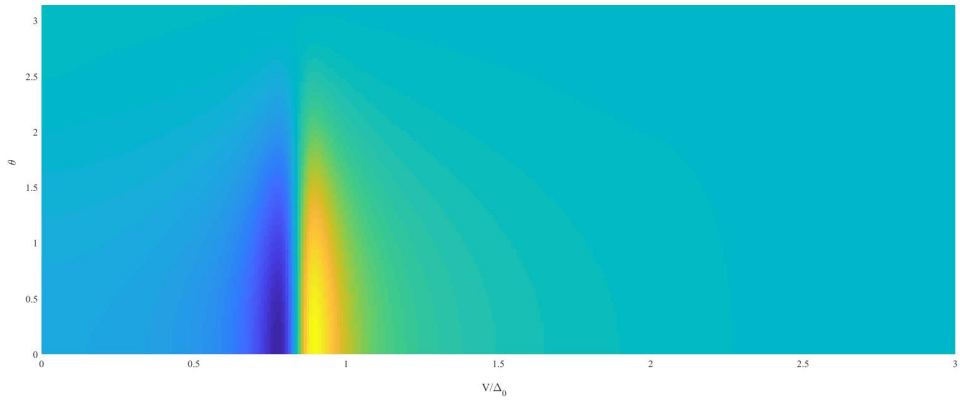

Figure 10.14: I_y in the plane of θ and V.

10.3.2 The α-dependence

Surface plots of the V and α-dependence is presented in the ensuing subsection. It has been shown that α can be used to control the transition to a π-junction, by the appliance of an external magnetic field [9]. Then, by applying a voltage bias to the system, introduces another mechanism by which the $0-\pi$ transition can be induced.

Figure 10.15 and 10.16 presents the charge-supercurrent as a function of α and V. It demonstrates how increasing values of α expedite the supercurrent peak with respect to the voltage. At $\alpha = \pi$, the maximum value of the charge-supercurrent is found at $V = 0$, whereas for $\alpha = 0$, the peak is at $V \sim 0.9\Delta_0$ as is clearly in figure 10.16. The analytical expression for I_Q in eq. (9.15) shows a partial dependence of α through a cosine function.

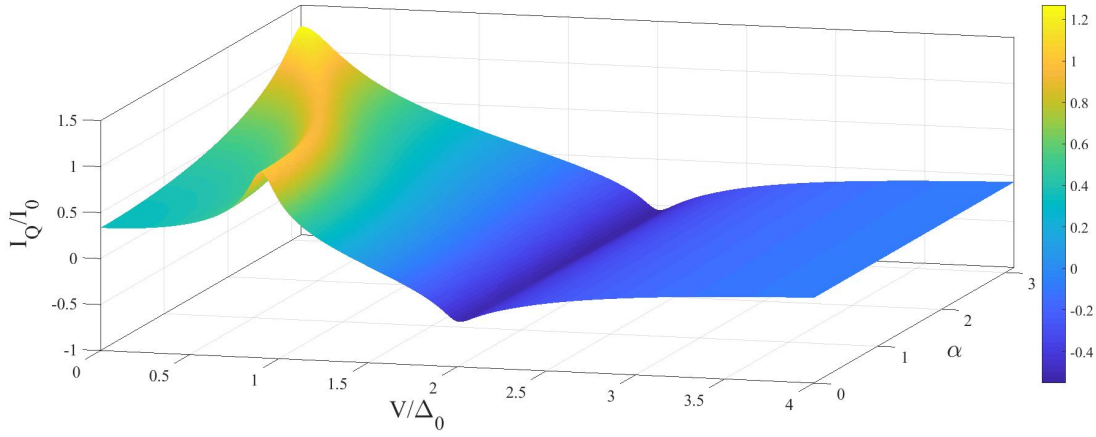

Figure 10.15: I_Q as a function of control voltage and displacement angle, α. $G_\phi = 1.5$, $\phi = \pi/3$, $\theta = \pi/2$, $d = 20$nm, $\xi_s = 30$nm, $T_c/T = 0.02$ and $\zeta = 5$.

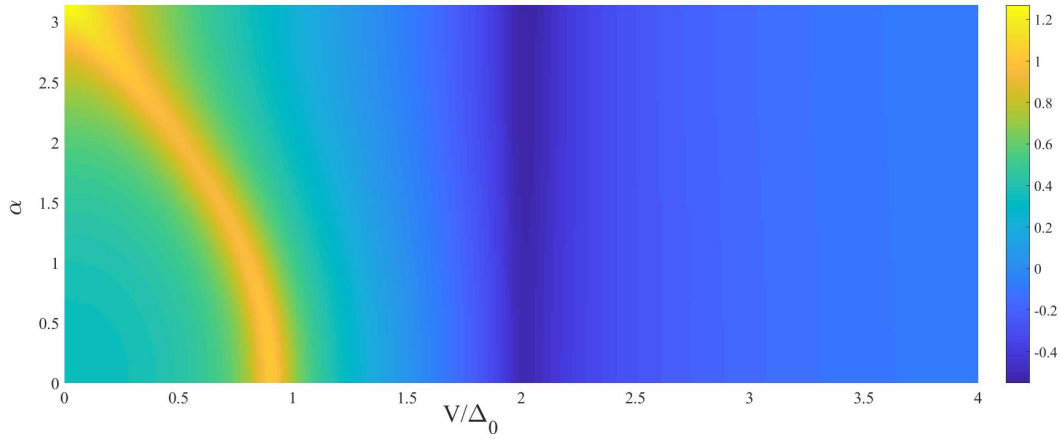

Figure 10.16: I_Q in the plane of control voltage V and displacement angle α. $G_\phi = 1.5$, $\phi = \pi/3$, $\theta = \pi/2$, $d = 20\text{nm}$, $\xi_s = 30\text{nm}$, $T_c/T = 0.02$ and $\zeta = 5$.

Presenting in figures 10.17 and 10.18 I_x as a function of V and α. The peak of the supercurrent is sharply followed by a decrease and change of sign, in contrast to the charge-supercurrent which decreases at a slower pace with respect to V. As mentioned above, this owes to the size of the spectral current of the spin-supercurrents, being much smaller than the charge-supercurrent. In addition is can be seen in figure 10.18, that for $\alpha = 0$, the spin-supercurrent is also zero, confirming the analytical expression for I_x presented in eq. (9.15) having a sine dependence on α.

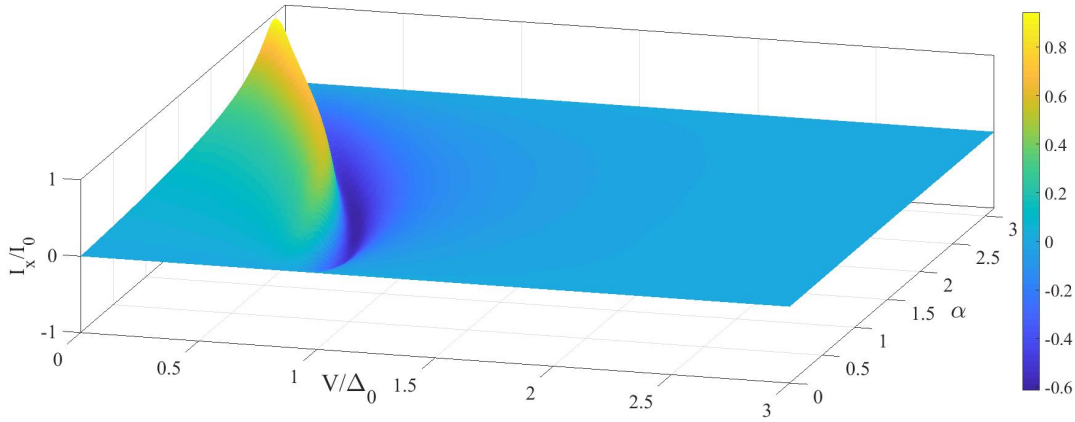

Figure 10.17: I_x as a function of control voltage and displacement angle, α. $G_\phi = 1.5$, $\phi = \pi/3$, $\theta = \pi/2$, $d = 20\text{nm}$, $\xi_s = 30\text{nm}$, $T_c/T = 0.02$ and $\zeta = 5$.

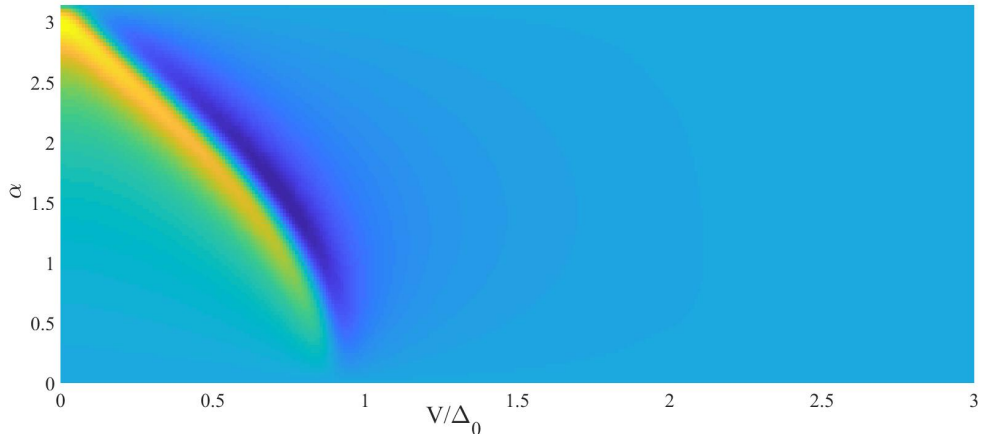

Figure 10.18: I_x in the plane of control voltage V and displacement angle α. $G_\phi = 1.5$, $\phi = \pi/3$, $\theta = \pi/2$, $d = 20$nm, $\xi_s = 30$nm, $T_c/T = 0.02$ and $\zeta = 5$.

Figures 10.19 and 10.20 shows I_y as a function of V and α. As is to be expected, its appearance is very similar to that of I_x vs V and α, but with the opposite sign, going from a negative value to a sharp increase to a peak, followed by a decrease to zero thereafter. Due to the same α-dependence as I_x, I_y is also zero for $\alpha = 0$.

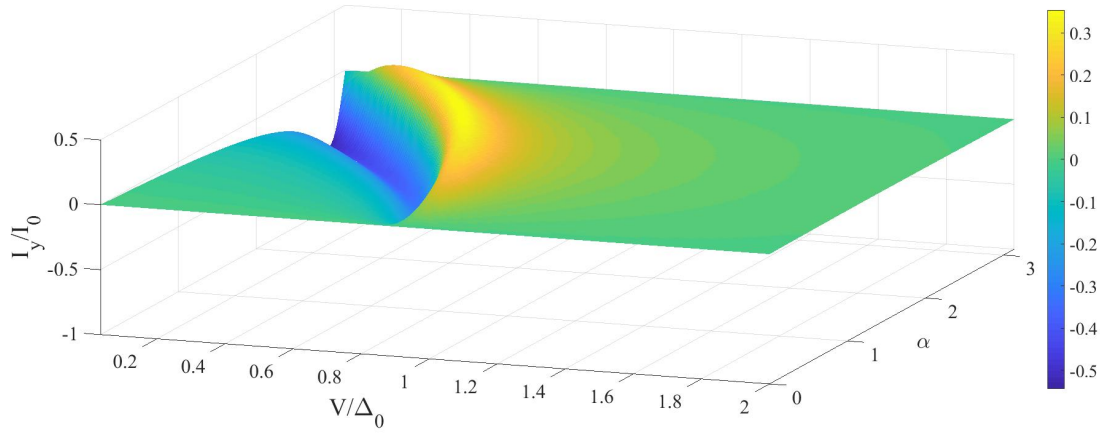

Figure 10.19: I_y as a function of control voltage and displacement angle, α. $G_\phi = 1.5$, $\phi = \pi/3$, $\theta = \pi/2$, $d = 20$nm, $\xi_s = 30$nm, $T_c/T = 0.02$ and $\zeta = 5$.

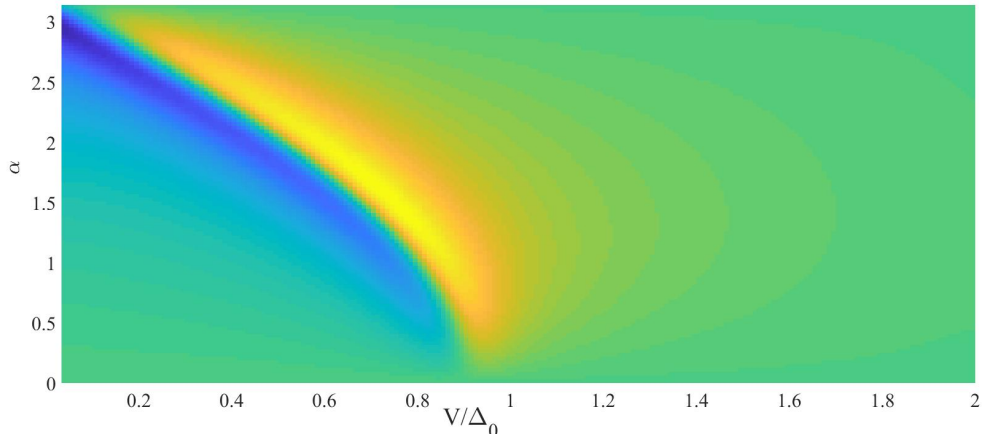

Figure 10.20: I_y in the plane of control voltage V and displacement angle α. $G_\phi = 1.5$, $\phi = \pi/3$, $\theta = \pi/2$, $d = 20\text{nm}$, $\xi_s = 30\text{nm}$, $T_c/T = 0.02$ and $\zeta = 5$.

Chapter 11

Conclusion

The quasiclassical theory of superconductivity has been applied to a spin-active Josephson junction, and it has been shown that the magnitude of the spin-supercurrents induced in a can be tuned by non-equilibrium effects in the normal metal, brought forth by the application of a voltage bias across the weak link. In addition can the transition from a $0 - \pi$ junction can be controlled via altering the voltage. The magnitude and the transition point of the supercurrents can be altered by the length of the normal metal, the transparency of the interface and the spin-mixing term, demonstrating that different set-ups can give different results and behaviours.

Being able to control spin-supercurrents with voltages offers great potential for the development of spin-transistors. The presence of voltage control in already existing semi-conductor technology makes the ability to control spin-supercurrents in future spintronic devices in a similar way, enticingly practical. This work shows that there is theoretical grounds for implementing voltage control in spintronic devises, pending that the field continues down the promising path it is on at present.

Bibliography

[1] , Jaroslav Fabian, and S. Das Sarma. "Spintronics: Fundamentals and applications". In: *Rev. Mod. Phys.* 76 (2 2004), pp. 323–410. DOI: 10.1103/RevModPhys.76.323. URL: https://link.aps.org/doi/10.1103/RevModPhys.76.323.

[2] F. Hübler et al. "Long-Range Spin-Polarized Quasiparticle Transport in Mesoscopic Al Superconductors with a Zeeman Splitting". In: *Phys. Rev. Lett.* 109 (20 2012), p. 207001. DOI: 10.1103/PhysRevLett.109.207001. URL: https://link.aps.org/doi/10.1103/PhysRevLett.109.207001.

[3] H. Yang , S.H. Yang, S. Takahashi,S. Maekawa and S. S. P. . Parkin. "Extremely long quasiparticle spin lifetimes in superconducting aluminium using MgO tunnel spin injectors". In: *Nature Materials* 9.586 (2010). DOI: |DOI:10.1038/NMAT2781.

[4] R. S. Keizer et al. "A spin triplet supercurrent through the half-metallic ferromagnet CrO_2". In: *Nature* 439 (Feb. 2006), pp. 825–827. DOI: 10.1038/nature04499.

[5] J. Linder and J. W. Robinson. "Superconducting Spintronics". In: *Nature Physics* 11 (2015), 307315. DOI: 0.1038/NPHYS3242.

[6] F. S. Bergeret , A. F. Volkov and K. B. Efetov. "Odd Triplet Superconductivity and Related Phenomena in Superconductor-Ferromagnet Structures". In: *Reviews of modern physics* (2005). DOI: 10.1103/RevModPhys.77.1321.

[7] A. Kadigrobov, R. I. Shekhter, and M. Jonson. "Quantum spin fluctuations as a source of long-range proximity effects in diffusive ferromagnet-super conductor structures". In: *EPL (Europhysics Letters)* 54.3 (2001), p. 394. URL: http://stacks.iop.org/0295-5075/54/i=3/a=394.

[8] M. Eschrig et al. "Theory of Half-Metal/Superconductor Heterostructures". In: *Phys. Rev. Lett.* 90 (13 2003), p. 137003. DOI: 10.1103/PhysRevLett.90.137003. URL: https://link.aps.org/doi/10.1103/PhysRevLett.90.137003.

[9] I. Gomperud and J. Linder. "Spin supercurrent and phase-tunable triplet Cooper pairs via magnetic insulators". 2015.

[10] F.K. Wilhelm, Gerd Schon and A.D. Zaikin. "Mesoscopic Superconducting - Normal Metal - Superconducting Transistor". In: *Physical Review Letters* 81.8 (1998).

[11] A.F. Morpurgo, T.M. Klapwjik and B.J. van Wees. "Hot electron tunable supercurrent". In: *Applied Physics Letters* 72.966 (8 1998). DOI: 10.1063/1.120612.

[12] H. Pothier et al. "Energy Distribution Function of Quasiparticles in Mesoscopic Wires". In: *Phys. Rev. Lett.* 79 (18 1997), pp. 3490–3493. DOI: 10.1103/PhysRevLett.79.3490. URL: https://link.aps.org/doi/10.1103/PhysRevLett.79.3490.

[13] P. M. Tedrow and R. Meservey. "Spin-Dependent Tunneling into Ferromagnetic Nickel". In: *Phys. Rev. Lett.* 26 (4 1971), pp. 192–195. DOI: 10.1103/PhysRevLett.26.192. URL: https://link.aps.org/doi/10.1103/PhysRevLett.26.192.

[14] P. M. Tedrow and R. Meservey. "Spin Polarization of Electrons Tunneling from Films of Fe, Co, Ni, and Gd". In: *Phys. Rev. B* 7 (1 1973), pp. 318–326. DOI: 10.1103/PhysRevB.7.318. URL: https://link.aps.org/doi/10.1103/PhysRevB.7.318.

[15] R. Meservey and P.M. Tedrow. "Spin-polarized electron tunneling". In: *Physics Reports* 238.4 (1994), pp. 173 –243. ISSN: 0370-1573. DOI: https://doi.org/10.1016/0370-1573(94)90105-8. URL: http://www.sciencedirect.com/science/article/pii/0370157394901058.

[16] Mark Johnson and R. H. Silsbee. "Interfacial charge-spin coupling: Injection and detection of spin magnetization in metals". In: *Phys. Rev. Lett.* 55 (17 1985), pp. 1790–1793. DOI: 10.1103/PhysRevLett.55.1790. URL: https://link.aps.org/doi/10.1103/PhysRevLett.55.1790.

[17] S.S. Saxena , P. Agarwal , F.M. Grosche ,R.K.W. Haselwimmer , M.J. Steiner , E. Pugh , I.R. Walker , S.R. Julian , P. Monthoux , G.G. Lonzarich , A. Huxley , I. Sheikin , D. Braithwaite and J. Flouquet. "Superconductivity on the border of itinerant-electron ferromagnetism in UGe2". In: *Nature* 406 (2000), pp. 587–592. DOI: 10.1038/35020500.

[18] D.Aoki and J. Flouquet. "Ferromagnetism and Superconductivity in Uranium Compounds". In: *Journal of the Physical Society of Japan* 81.1 (2012), p. 011003. DOI: 10.1143/JPSJ.81.011003. URL: https://doi.org/10.1143/JPSJ.81.011003.

[19] A. I. Buzdin. "Proximity effects in superconductor-ferromagnet heterostructures". In: *Rev. Mod. Phys.* 77 (3 2005), pp. 935–976. DOI: 10.1103/RevModPhys.77.935. URL: https://link.aps.org/doi/10.1103/RevModPhys.77.935.

[20] Michael Tinkham. *Introduction to Superconductivity*. 1975.

[21] D. van Delft and P. Kes. "The discovery of superconductivity". In: *Physics Today* 63 (2010), pp. 38–43. DOI: 10.1063/1.3490499.

[22] H. Kamerlingh-Onnes. “Further experiments with liquid helium. D. On the change of electric resistance of pure metals at very low temperatures, etc. V. The disappearance of the resistance of mercury.” In: *Commun. Phys. Lab. Univ. Leiden* 122b (1911).

[23] W. Meissner and R. Oschenfeld. “Ein neuer Effekt bei Eintritt der Supraleitfhigkeit”. In: *Naturwiss* 21 (), p. 787.

[24] F. and H. London. “The Electromagnetic equations of the Supraconductor”. In: *The Royal Society* (1935).

[25] V.L. Ginzburg and L. D. Landau. “On the Theory of superconductivity”. In: *Zh.Eksp.Teor.Fiz.* 20 (1950), pp. 1064–1082.

[26] J. Bardeen, L. N. Cooper and J. R. Schrieffer. “Theory of Superconductivity”. In: *Physical Review Journals* (1957).

[27] L. P. Gor’kov. “On the energy spetrum of superconductors”. In: *Soviet physics JETP* 34.3 (1958), pp. 735–739.

[28] Leon N. Cooper. “Bound Electron Pairs in a Degenerate Fermi Gas”. In: *Physical Review Journals* (1956).

[29] Matthias Eschrig. “Spin-polarized supercurrents for spintronics”. In: *Physics Today* (2011).

[30] A. Zagoskin. *Quantum Theory of Many-Body Systems*. Springer, 2014.

[31] A. L. Fetter and J. D. Walecka. *Quantum Theory of Many-Particle Systems*. 2003, p. 443.

[32] Gerald D. Mahan. *Many-particle Physics*. Third. Kluwer Academic/Plenum Publishers, 2000.

[33] J.W Serene and D Rainer. “The quasiclassical approach to superfluid 3He”. In: *Physics Reports* 101.4 (1983), pp. 221 –311. ISSN: 0370-1573. DOI: https://doi.org/10.1016/0370-1573(83)90051-0. URL: http://www.sciencedirect.com/science/article/pii/0370157383900510.

[34] J. Rammer, H. Smith. “Quantum field-theoretical methods in transport theory of metals”. In: *Reviews of Modern Physics, Vol. 58, No. 2* (1986).

[35] J. P. Morten. “Spin and charge transport in dirty superconductors”. 2003.

[36] M. Amundsen. “Quasiclassical Theory Beyond 1D: Supercurrents and Topological Excitations”. Master thesis. Norwegian University of Science and Technology, 2016.

[37] P. Muller and A.V. Ustinov. *The Physics of Superconductors*. Springer, 1997.

[38] R. D. Mattuck. *A Guide to Feynman Diagrams in the Many-Body Problem*. McGraw-Hill Publishing, 1967.

[39] K. F. Riley , M. P. Hobson and S. J. Bence. *Mathematical methods for physics and engineering*. 3rd. Cambridge, 2006.

[40] B. D. Josephson. “Possible new effects in superconductive tunnelling”. In: *Physics Letters* 1.7 (1962).

[41] Asle Sudb Kristian Fossheim. *Superconductivity, Physics and Applications*. 2004.

[42] D. Sprungmann et al. “Evidence for triplet superconductivity in Josephson junctions with barriers of the ferromagnetic Heusler alloy Cu_2MnAl”. In: *Phys. Rev. B* 82 (6 2010), p. 060505. DOI: 10.1103/PhysRevB.82.060505. URL: https://link.aps.org/doi/10.1103/PhysRevB.82.060505.

[43] J.W.A. Robinson, J.D.S. Witt and M. G. Blamire. “Controlled Injection of Spin-Triplet Supercurrents into a Strong Ferromagnet”. In: *Science* 329 (5987 2010), pp. 59–61. DOI: 10.1126/science.1189246.

[44] Trupti S. Khaire et al. “Observation of Spin-Triplet Superconductivity in Co-Based Josephson Junctions”. In: *Phys. Rev. Lett.* 104 (13 2010), p. 137002. DOI: 10.1103/PhysRevLett.104.137002. URL: https://link.aps.org/doi/10.1103/PhysRevLett.104.137002.

[45] Bin Li et al. “Superconducting Spin Switch with Infinite Magnetoresistance Induced by an Internal Exchange Field”. In: *Phys. Rev. Lett.* 110 (9 2013), p. 097001. DOI: 10.1103/PhysRevLett.110.097001. URL: https://link.aps.org/doi/10.1103/PhysRevLett.110.097001.

[46] L. Trifunovic. “Long-Range Superharmonic Josephson Current”. In: *Phys. Rev. Lett.* 107 (4 2011), p. 047001. DOI: 10.1103/PhysRevLett.107.047001. URL: https://link.aps.org/doi/10.1103/PhysRevLett.107.047001.

[47] Y. V. Nazarov. “Novel circuit theory of Andreev reflection”. In: *Superlattices and Microstructures* 25 (5-6 1999), pp. 1221–1231.

[48] M. Yu. Kuprianov and V. F. Lukichev. “Influence of boundary transparency on the critical current of "dirty" SS'S structures”. In: *JETP, Vol. 67, No. 6, p. 1163* (1988).

[49] A. Cottet, D. Huertas-Hernando, W. Belzig and Y. V. Nazarov. “Spin dependent boundary conditions for isotropic superconducting Green's functions”. In: *Physical Review* 80.184511 (2009).

[50] W. Belzig, F.K. Wilhelm, C. Bruder and G. Schon. “Quasiclassical Greens function approach to mesoscopic superconductivity”. In: *Superlattices and Microstructures* 25.5/6 (1999).

[51] V. Chandrasekhar. “An introduction to the quasiclassical theory of superconductivity for diffusive proximity-coupled systems”. In: *arXiv:cond-mat* (2008).

Appendix A

On the derivation of the equation of motion

The explicit derivation of eq. (3.28a) and (3.28b) is showed in this appendix. It follows the derivation done by J. P. Morten[35] in 2003. The same procedure holds for the advanced Green's function, so no explicit run-through is given for it. The derivation for the Keldysh Green's function is included below, as it does not contain the step function, and the derivation is therefore slightly different. For the retarded and advanced Green's functions, the derivation takes the following form:

$$
\begin{aligned}
\Big(i\hbar\partial_{t_1}\hat{\rho}_3 G^R(1,2)\Big)_{ij} &= \sum_k i\partial_{t_1}(\hat{\rho}_3)_{ik}\big(\hat{G}^R(1,2)\big)_{kj} \\
&= \sum_{kl} i\partial_{t_1}(\hat{\rho}_3)_{ik}(-\Theta(t_1-t_2))(\hat{\rho}_3)_{kl}\Big\langle\big\{(\psi(1))_l,(\psi^\dagger(2))_j\big\}\Big\rangle \\
&= \sum_{kl}\delta(t_1-t_2)(\hat{\rho}_3)_{ik}(\hat{\rho}_3)_{kl}\Big\langle\big\{(\psi(1))_l,(\psi^\dagger(2))_j\big\}\Big\rangle \\
&\quad + \sum_{kl}(-i\Theta(t_1-t_2))(\hat{\rho}_2)_{kl}\Big\langle\big\{i\partial_{t_1}(\hat{\rho}_3)_{ik}(\psi(1))_l,(\psi^\dagger(2))_j\big\}\Big\rangle \\
&= \sum_l \delta(t_1-t_2)\delta_{il}\delta_{lj}\delta(\boldsymbol{r_1}-\boldsymbol{r_2}) \\
&\quad + \sum_l(-i\Theta(t_1-t_2))(\hat{\rho}_3)_{ll}\Big\langle\big\{(\hat{H}(1))_{il}(\psi(1))_l,(\psi^\dagger(2))_j\big\}\Big\rangle \\
&= \delta_{ij}\delta(1-2) \\
&\quad + \sum_l(\hat{H}(1))_{il}(-i\Theta(t_1-t_2))(\hat{\rho}_3)_{ll}\Big\langle\big\{(\psi(1))_l,(\psi^\dagger(2))_j\big\}\Big\rangle \\
&= \delta_{ij}\delta(1-2) + \big(\hat{H}(1)\hat{G}^R\big)_{ij}.
\end{aligned}
\tag{A.1}
$$

The commutation relations for the field operators, defined in eq. (1.6) are used, and the matrix representation of the equation of motion for the field operator $\psi(1)$ from eq. (3.25):

$$
\sum_l i\partial_{t_1}(\hat{\rho}_3)_{il}(\psi(1))_l = \sum_l(\hat{H}(1))_{il}(\psi(1))_l, \tag{A.2}
$$

are used. For the Keldysh component G^K defined in eq. (2.4c), the procedure is:

$$
\begin{aligned}
\Big(\big(i\partial_{t_1}\hat{\rho}_3\hat{G}^K(1,2)\big)\Big)_{ij} &= \sum_k i\partial_{t_1}(\hat{\rho}_3)_{ik}\big(\hat{G}^K(1,2)\big)_{kj} \\
&= \sum_{kl} i\partial_{t_1}(\hat{\rho}_3)_{ik}(-i)(\hat{\rho}_3)_{kl}\Big\langle\, [\,(\psi(1))_l, (\psi^\dagger(2))_j]\,\Big\rangle \\
&= \sum_{kl}(-i)(\hat{\rho}_3)_{kl}\Big\langle\, \big[i\partial_{t_1}(\hat{\rho}_3)_{ik}(\psi(1))_l, (\psi^\dagger(2))_j\big]\,\Big\rangle \\
&= \sum_{l}(-i)(\hat{\rho}_3)_{ll}\Big\langle\, \big[(\hat{H})_{il}(\psi(1))_l, (\psi^\dagger(2))_j\big]\,\Big\rangle \\
&= \sum_{l}(\hat{H}(1))_{il}(-i)(\hat{\rho}_3)_{ll}\Big\langle\, (\psi(1))_l, (\psi^\dagger(2))_j\,\Big\rangle \\
&= \big(\hat{H}(1)\hat{G}^K(1,2)\big)_{ij}
\end{aligned}
\tag{A.3}
$$

Appendix B

Derivaton of the current expression

Deriving an expression for the charge and spin currents for the system starts with basic quantum mechanics. The derivation follows the work of M. Amundsen [36], and J.P. Morten [35]. The expression for the spatial probability charge density is:

$$\rho_e(\boldsymbol{r},t) = e|\psi(\boldsymbol{r},t)|^2 = e\big\langle\psi^\dagger(\boldsymbol{r},t)\psi(\boldsymbol{r},t)\big\rangle. \tag{B.1}$$

The particle density is related to the current density through the continuity equation:

$$\partial_t\rho_e(\boldsymbol{r},t) + \nabla\cdot\boldsymbol{J}_e(\boldsymbol{r},t) = 0, \tag{B.2}$$

and time-derivative of the particle density is found with the use of the Schrodinger equation:

$$\begin{aligned}
\partial_t\rho_e(\boldsymbol{r},t) &= e\,\partial_t\big\langle\psi^\dagger(\boldsymbol{r},t)\psi(\boldsymbol{r},t)\big\rangle \\
&= e\,\big\langle\partial_t\psi^\dagger(\boldsymbol{r},t)\psi(\boldsymbol{r},t) + \psi^\dagger(\boldsymbol{r},t)\partial_t\psi(\boldsymbol{r},t)\big\rangle \\
&= -\frac{ie\hbar}{2m}\big\langle\big(\nabla + \frac{i}{\hbar}\boldsymbol{A}(\boldsymbol{r},t)\big)^2\psi^\dagger(\boldsymbol{r},t)\psi(\boldsymbol{r},t) \\
&\qquad\qquad - \psi^\dagger\big(\nabla - \frac{i}{\hbar}\boldsymbol{A}(\boldsymbol{r},t)\big)^2\psi(\boldsymbol{r},t)\big\rangle \\
&= -\nabla\frac{ie\hbar}{2m}\big\langle\big(\nabla + \frac{i}{\hbar}\boldsymbol{A}(\boldsymbol{r},t)\big)\psi^\dagger(\boldsymbol{r},t)\psi(\boldsymbol{r},t) \\
&\qquad\qquad - \psi^\dagger(\boldsymbol{r},t)\big(\nabla - \frac{i}{\hbar}\boldsymbol{A}(\boldsymbol{r},t)\big)\psi(\boldsymbol{r},t)\big\rangle.
\end{aligned} \tag{B.3}$$

Inserting this into eq. (B.2) and involving spin:

$$\boldsymbol{J}_e(\boldsymbol{r},t) = \frac{ie\hbar}{2m}\sum_\sigma \big\langle \big(\nabla + \frac{i}{\hbar}\boldsymbol{A}(\boldsymbol{r},t)\big)\psi^\dagger_\sigma(\boldsymbol{r},t)\psi_\sigma(\boldsymbol{r},t) - \psi^\dagger_\sigma(\boldsymbol{r},t)\big(\nabla - \frac{i}{\hbar}\boldsymbol{A}(\boldsymbol{r},t)\big)\psi_\sigma(\boldsymbol{r},t)\big\rangle \tag{B.4}$$

The objective is to express the current in terms of Green's functions. Appreciating the fact that the relevant Greens functions are two-particle functions, with different spatial coordinates $(1) = (\boldsymbol{r_1}, t)$ and $(2) = (\boldsymbol{r}_2, t)$, and expression (B.5) taken as the limit at which the two particles are located in the same place $1 \to 2$, the current can be written out as such:

$$\begin{aligned}\boldsymbol{J}_e(1) &= \lim_{1\to 2}\frac{ie\hbar}{2m}\sum_\sigma \big\langle \big(\nabla_2 + \frac{i}{\hbar}\boldsymbol{A}(2)\big)\psi^\dagger_\sigma(2)\psi_\sigma(1) \\ &- \psi^\dagger_\sigma(2)\big(\nabla_2 - \frac{i}{\hbar}\boldsymbol{A}(2)\big)\psi_\sigma(1)\big\rangle \\ &= \lim_{1\to 2}\frac{ie\hbar}{2m}\sum_\sigma \big(\nabla_1 - \nabla_2 - \frac{i}{\hbar}\boldsymbol{A}_1 + \frac{i}{\hbar}\boldsymbol{A}_2\big)\big\langle\psi^\dagger_\sigma(2)\psi_\sigma(1)\big\rangle\end{aligned} \tag{B.5}$$

Where the expectation value can be written in terms of the Greens function:

$$\big\langle\psi^\dagger_\sigma(2)\psi_\sigma(1)\big\rangle = \frac{1}{2}\big\langle[\psi^\dagger_\sigma(2)\psi_\sigma(1)]\big\rangle + \frac{1}{2}\delta(1-2) = -\frac{i}{2}\hat{G}^K_{\sigma\sigma}(1,2) + \frac{1}{2}\hat{\rho}_0\delta(1-2)$$

(B.6a)

Owing to the fact that the electrons never really occupy the same position in space, the delta function will always be zero. Therefore, it is neglected, and the expression for the charge current in terms of the Greens function is then:

$$\boldsymbol{J}_e(1) = \lim_{1\to 2} -\frac{e\hbar}{4m}\mathrm{Tr}\Big\{\nabla_1 - \nabla_2 - \frac{i}{\hbar}\boldsymbol{A}(1) - \frac{i}{\hbar}\boldsymbol{A}(2)\Big\}\hat{G}^K_{\sigma\sigma}(1,2) \tag{B.7}$$

Approximating the current to the quasiclassical realm requires the Fourier transform of the current:

$$\begin{aligned}\boldsymbol{J}_e(\boldsymbol{R}) &= \lim_{\boldsymbol{r}\to 0} -\frac{e\hbar}{4m}\mathrm{Tr}\Big\{\big(\nabla_1 - \nabla_2 - \frac{i}{\hbar}\boldsymbol{A}(1) \\ &\qquad - \frac{i}{\hbar}\boldsymbol{A}(2)\big)\int\frac{dE}{2\pi}e^{-iEt/\hbar}\int\frac{d\boldsymbol{p}}{(2\pi)^3}e^{i\boldsymbol{p}\cdot\boldsymbol{r}/\hbar}\hat{G}^K(\boldsymbol{R},T,\boldsymbol{p},E)\Big\} \\ &= -\frac{e}{4\pi m}\int dE\int\frac{d\boldsymbol{p}}{(2\pi)^3}\big(\frac{i\boldsymbol{p}}{\hbar} - \frac{i}{\hbar}(\boldsymbol{A}(1)+\boldsymbol{A}(2)\big)\hat{G}^K(\boldsymbol{R},T,\boldsymbol{p},E) \\ &= -\frac{e}{4\pi m}N_0\int dE\ \mathrm{Tr}\Big\{\int\frac{d\Omega}{4\pi}(\boldsymbol{p}_F - \boldsymbol{A}(\boldsymbol{R}))\hat{g}^K(\boldsymbol{R},T,\boldsymbol{p},E)\Big\} \\ &= \frac{N_0 De}{4\hbar}\int dE\ \mathrm{Tr}\Big\{(\hat{g}\nabla\hat{g})^K\Big\} + \frac{N_0 e}{4\hbar m}\int dE\ \mathrm{Tr}\Big\{\boldsymbol{A}\hat{g}^K\Big\}\end{aligned} \tag{B.8}$$

Expanding for the inclusion of holes in the expression (B.8), which manifests as a hole-current flowing in the opposite direction as the particle-current, $\hat{\rho}_3$ is introduced into the expression:

$$\boldsymbol{J}_e = \frac{N_0 e\mathcal{D}}{4\hbar}\int dE\ \mathrm{Tr}\Big\{\hat{\rho}_3(\check{g}\nabla\check{g})^K\Big\} + \frac{N_{0e}}{4m\hbar}\int dE\ \mathrm{Tr}\Big\{\hat{\rho}_3\hat{\boldsymbol{A}}\hat{g}^K\Big\} \tag{B.9}$$

where the last term can be neglected due it being imaginary, and not physically observable. The expression for the current is then:

$$\boldsymbol{J}_e = \frac{N_0 e\mathcal{D}}{4\hbar}\int dE\ \mathrm{Tr}\Big\{\hat{\rho}_3(\check{g}\nabla\check{g})^K\Big\} \tag{B.10}$$

This is the expression for the charge current. It carries no information about the spin flow through the system. The spin-currents can be derived in the same way as the charge current, where the spin density is used:

$$\boldsymbol{\rho_s} = \frac{\hbar}{2}\sum_{\sigma\sigma'}\langle\psi^\dagger_\sigma\boldsymbol{\tau}_{\sigma\sigma'}\psi_{\sigma'}\rangle \tag{B.11}$$

The expressions for the spin-currents then become:

$$\boldsymbol{J}_s^x = \frac{N_0\mathcal{D}}{8}\int dE\ \mathrm{Tr}\left\{\hat{\rho}_3\hat{\tau}_x(\check{g}\nabla\check{g})^K\right\} \tag{B.12a}$$

$$\boldsymbol{J}_s^y = \frac{N_0\mathcal{D}}{8}\int dE\ \mathrm{Tr}\left\{\hat{\rho}_3\hat{\tau}_y(\check{g}\nabla\check{g})^K\right\} \tag{B.12b}$$

$$\boldsymbol{J}_s^z = \frac{N_0\mathcal{D}}{8}\int dE\ \mathrm{Tr}\left\{\hat{\rho}_3\hat{\tau}_z(\check{g}\nabla\check{g})^K\right\} \tag{B.12c}$$